

DTIC FILE COPY

0

AD-A218 277

ATMOSPHERIC WIND MEASUREMENTS USING A 50 MHZ
IMAGING DOPPLER INTERFEROMETER
RADAR

by

Michael Jerome Volek

A thesis submitted in partial fulfillment
of the requirements for the degree

of

MASTER OF SCIENCE

in

Soil Science and Biometeorology
(Aeronomy)

DTIC
S ELECTE D
FEB 23 1990
D

Approved:

Jane W. Anderson
Major Professor

Marique L. Loeberic by David Engstrom
Committee Member

Kent L. Miller
Committee Member

Lawrence H. Fietle
Dean of Graduate Studies

UTAH STATE UNIVERSITY
Logan, Utah

1989

DISTRIBUTION STATEMENT A
Approved for public release;
Distribution Unlimited

BEST
AVAILABLE COPY

90 02 21 059

REPORT DOCUMENTATION PAGE

Form Approved
OMB No. 0704-0188

1a. REPORT SECURITY CLASSIFICATION UNCLASSIFIED		1b. RESTRICTIVE MARKINGS NONE	
2a. SECURITY CLASSIFICATION AUTHORITY		3. DISTRIBUTION / AVAILABILITY OF REPORT APPROVED FOR PUBLIC RELEASE; DISTRIBUTION UNLIMITED.	
2b. DECLASSIFICATION / DOWNGRADING SCHEDULE			
4. PERFORMING ORGANIZATION REPORT NUMBER(S)		5. MONITORING ORGANIZATION REPORT NUMBER(S) AFIT/CI/CIA- 89-049	
6a. NAME OF PERFORMING ORGANIZATION AFIT STUDENT AT UTAH STATE UNIVERSITY	6b. OFFICE SYMBOL <i>(if applicable)</i>	7a. NAME OF MONITORING ORGANIZATION AFIT/CIA	
6c. ADDRESS (City, State, and ZIP Code)		7b. ADDRESS (City, State, and ZIP Code) Wright-Patterson AFB OH 45433-6583	
8a. NAME OF FUNDING / SPONSORING ORGANIZATION	8b. OFFICE SYMBOL <i>(if applicable)</i>	9. PROCUREMENT INSTRUMENT IDENTIFICATION NUMBER	
8c. ADDRESS (City, State, and ZIP Code)		10. SOURCE OF FUNDING NUMBERS	
		PROGRAM ELEMENT NO.	PROJECT NO.
		TASK NO.	WORK UNIT ACCESSION NO.
11. TITLE (Include Security Classification) (UNCLASSIFIED) Atmospheric Wind Measurements Using a 50 MHz Imaging Doppler Interferometer Radar			
12. PERSONAL AUTHOR(S) Michael Jerome Volek			
13a. TYPE OF REPORT THESIS / DISSEMINATION	13b. TIME COVERED FROM _____ TO _____	14. DATE OF REPORT (Year, Month, Day) 1989	15. PAGE COUNT 92
16. SUPPLEMENTARY NOTATION APPROVED FOR PUBLIC RELEASE IAW AFR 190-1 ERNEST A. HAYGOOD, 1st Lt, USAF Executive Officer, Civilian Institution Programs			
17. COSATI CODES		18. SUBJECT TERMS (Continue on reverse if necessary and identify by block number)	
FIELD	GROUP	SUB-GROUP	
19. ABSTRACT (Continue on reverse if necessary and identify by block number)			
20. DISTRIBUTION / AVAILABILITY OF ABSTRACT <input checked="" type="checkbox"/> UNCLASSIFIED/UNLIMITED <input type="checkbox"/> SAME AS RPT. <input type="checkbox"/> DTIC USERS		21. ABSTRACT SECURITY CLASSIFICATION UNCLASSIFIED	
22a. NAME OF RESPONSIBLE INDIVIDUAL ERNEST A. HAYGOOD, 1st Lt, USAF		22b. TELEPHONE (Include Area Code) (513) 255-2259	22c. OFFICE SYMBOL AFIT/CI

ACKNOWLEDGEMENTS

This research was supported by the National Science Foundation under grants ATM-8608391, ATM-8719781, and ATM-8813454; by the United States Air Force Office of Scientific Research under contract number F49620-89-C-022, and by a grant from Holodyne, Inc. I would also like to thank the U. S. Air Force for providing me this opportunity to attend graduate school under the Air Force Institute of Technology program.

I would like to express my appreciation to Dr. Gene W. Adams for all his help and guidance throughout the course of this research. I also appreciate the opportunity that he gave me to conduct this research. I would also like to express my thanks to my other committee members, Dr. Kent L. Miller and Dr. Monique Y. Leclerc, for their helpful comments and suggestions concerning this effort; to Mr. John Brosnahan of Tycho Technology, Inc., for his tour of the MENTOR site; to Dr. Vern Peterson, also of Tycho Technology, Inc., for obtaining the LaSalle rawinsonde and Platteville ST data; to the United States Air Force Environmental Technical Applications Center for providing the Denver rawinsonde and HIRAS data; to fellow graduate student Ali Ghafourian, who not only helped immensely with much of the filtering software, but acted as a sounding board for many suggestions on how to analyze the data; and to Teri Olsen for her help in preparing the manuscript.

Last, but not least, I would like to thank my wife, Stacy, and my daughter, Anastasia, for their love and support during the course of my research. Even though Stacy was pregnant with twins during the final stages of this effort, she still took care of everything, providing me with the time I needed to complete this work.

Michael Jerome Volek

Accession For	
NTIS CRA&I	<input checked="" type="checkbox"/>
DTIC TAB	<input type="checkbox"/>
Unannounced	<input type="checkbox"/>
Justification	
By	
Distribution/	
Availability Codes	
Data	Availability for Special
A-1	



TABLE OF CONTENTS

	Page
ACKNOWLEDGEMENTS	ii
LIST OF FIGURES	v
ABSTRACT	viii
Chapter	
I. INTRODUCTION	1
II. LITERATURE REVIEW	7
Imaging Doppler Interferometry	18
III. DATA ANALYSIS	25
The MENTOR 50 MHz IDI Radar	25
Tropospheric Wind Analysis	27
IV. RESULTS AND DISCUSSION	52
V. CONCLUSIONS AND RECOMMENDATIONS	80
REFERENCES	83
APPENDIX	86

LIST OF FIGURES

Figure	Page
1. Various atmospheric wind measurement techniques (From Gage and Van Zandt, 1981)	5
2. Plot of spectral power density vs. Doppler shift (From Balsley, 1978)	14
3. Geometry for single horizontally moving target being viewed by a two-antenna interferometer (From Adams et al., 1985)	20
4. Complex Fourier spectra for the two antennas in Figure 3, showing the signature of a single moving target (From Adams et al., 1985)	21
5. The MENTOR set-up	26
6. MENTOR system block diagram	29
7. Wind component input to synthetic data generator	31
8. Test calculations using synthetic data and 10 points per velocity	32
9. Test calculations using synthetic data and 15 points per velocity	33
10. Test calculations using synthetic data and 30 points per velocity	34
11. Test calculations using synthetic data and 60 points per velocity	35
12. Scatter plot of radial zenith angle vs. radial velocity from 10 minutes of MENTOR data	41
13. Scatter plot of E-W zenith angle vs. altitude from MENTOR	44
14. Scatter plot of N-S zenith angle vs. altitude from MENTOR	45
15. Scatter plot of E-W received voltage vs. E-W zenith angle from MENTOR	46
16. Scatter plot of N-S received voltage vs. N-S zenith angle from MENTOR	47

Figure	Page
17. Scatter plot of E-W received voltage vs. altitude from MENTOR	48
18. Scatter plot of N-S received voltage vs. altitude from MENTOR	49
19. A comparison of horizontal wind speeds determined by the 18:25:10-18:35:10 MENTOR data, the LaSalle rawinsondes, and the Platteville ST radar	55
20. A comparison of horizontal directions determined by the 18:25:10-18:35:10 MENTOR data, the LaSalle rawinsondes, and the Platteville ST radar	56
21. A comparison of zonal wind speeds determined by the 18:25:10-18:35:10 MENTOR data, the LaSalle rawinsondes, and the Platteville ST radar	57
22. A comparison of meridional wind speeds determined by the 18:25:10-18:35:10 MENTOR data, the LaSalle rawinsondes, and the Platteville ST radar	58
23. A comparison of horizontal wind speeds determined by the 18:25:10-18:35:10 MENTOR data and the Denver rawinsondes	60
24. A comparison of horizontal directions determined by the 18:25:10-18:35:10 MENTOR data and the Denver rawinsondes	61
25. A comparison of zonal wind speeds determined by the 18:25:10-18:35:10 MENTOR data and the Denver rawinsondes	62
26. A comparison of meridional wind speeds determined by the 18:25:10-18:35:10 MENTOR data and the Denver rawinsondes	63
27. A comparison of vertical velocities determined by the MENTOR 18:25:10-18:35:10 data and the AFGWC HIRAS model for Denver	65
28. Plot of baroclinicity vs. altitude from the MENTOR 18:25:10-18:35:10 data	66
29. A comparison of horizontal wind speeds determined by the MENTOR 18:45:10-18:55:10 data, the LaSalle rawinsondes, and the Platteville ST radar	67

Figure	Page
30. A comparison of horizontal directions determined by the MENTOR 18:45:10-18:55:10 data, the LaSalle rawinsondes, and the Platteville ST radar	68
31. A comparison of zonal wind speeds determined by the MENTOR 18:45:10-18:55:10 data, the LaSalle rawinsondes, and the Platteville ST radar	69
32. A comparison of meridional wind speeds determined by the MENTOR 18:45:10-18:55:10 data, the LaSalle rawinsondes, and the Platteville ST radar	70
33. A comparison of horizontal wind speeds determined by the MENTOR 18:45:10-18:55:10 data and the Denver rawinsondes	72
34. A comparison of horizontal directions determined by the MENTOR 18:45:10-18:55:10 data and the Denver rawinsondes	73
35. A comparison of zonal wind speeds determined by the MENTOR 18:45:10-18:55:10 data and the Denver rawinsondes	74
36. A comparison of meridional wind speeds determined by the MENTOR 18:45:10-18:55:10 data and the Denver rawinsondes	75
37. A comparison of vertical velocities determined by the MENTOR 18:45:10-18:55:10 data and the AFGWC HIRAS model for Denver	77
38. Plot of baroclinicity vs. altitude from the MENTOR 18:45:10-18:55:10 data	78

ABSTRACT

Atmospheric Wind Measurements Using
a 50 MHz Imaging Doppler Interferometer Radar

by

Michael Jerome Volek, Master of Science
Utah State University

Major Professor: Dr. Gene W. Adams
Department: Soil Science and Biometeorology

→ The 50 megahertz radar located near LaSalle, Colorado, also known as MENTOR, was operated as an Imaging Doppler Interferometer (IDI) in order to collect radar data. These data were collected from 18:25 Universal Time to 20:15 Universal Time on 14 October 1988. The data were used to measure winds in the lower atmosphere from less than 1 kilometer up to approximately 11.25 kilometers. The raw data were transformed from time domain to frequency domain so that the IDI technique could be employed. The number of returns decreased with altitude, as did their radial distance off-zenith. Filters were developed to reject points that did not meet certain criteria, and then algorithms were developed to derive wind speeds and directions. → The horizontal wind and its zonal and meridional components were compared to rawinsonde data gathered at the radar site concurrently with the IDI measurements, to data gathered from

the ST (stratosphere-troposphere) radar at Platteville, Colorado, and to the 14 Oct/12:00 UT and 15 Oct/00:00 UT rawinsonde runs at Denver. The vertical velocities measured were compared to vertical velocities derived from the Air Force Global Weather Central (AFGWC) High Resolution (HIRAS) model for Denver. Also, baroclinicity values were derived from the MENTOR data and plotted as a function of altitude.

(101 pages)

CHAPTER I

INTRODUCTION

Scientists have long been interested in atmospheric winds for various reasons. At first, they were an important consideration in weather forecasting. Today, however, the scope of importance of atmospheric winds is much broader as man utilizes the atmosphere in various ways. Commercial and military aviation, the Space Shuttle, ballistic missiles, and many other applications depend on the atmospheric winds, and the ability to determine the atmospheric wind structure is critical to the success of these systems. Errors in wind measurement can have tragic and costly results. For example, commercial airlines need wind data from the lower atmosphere in order to safely and economically plan their routes. That is why many new methods of instrumentation are being developed--to help meet the growing need for atmospheric wind data.

Man has used many different methods to sample the upper air winds. The first was by using a rawinsonde, which involves attaching a telemetering system to a balloon, then using simple trigonometry to calculate the winds (Byers, 1974). The upper limit of the rawinsonde is 36 km. Some innovative design changes in the balloon resulted in the Jimsphere, a balloon that is overfilled so that it expands on ascent. Jimspheres can remain aloft at fixed altitudes and telemeter wind information to ground sites. Their upper

limit is 27 km. After their development, rockets were used to gather wind data from regions inaccessible to balloons. Scientists could now sample the upper atmosphere up to 240 km (Byers, 1974).

Radar was a technological breakthrough that was of great benefit to atmospheric scientists. Incoherent scatter radars measure the plasma bulk flow of the upper atmosphere by sensing weakly re-radiated energy from upper atmospheric free electrons. The radar then measures the frequency change due to the Doppler shift, and then this frequency change can be used to measure radial velocities. Various techniques can then be employed to determine the horizontal and vertical velocities. This type of radar can only receive returns from ionospheric heights (above 60 km). The mesosphere-stratosphere-troposphere radar (MST) uses a large, coherent, monostatic radar operating in the VHF-UHF range to obtain echoes in the optically clear atmosphere from 1-100 km (Balsley, 1981). The primary echoing mechanism involves scattering from turbulent irregularities having a scale size equal to one-half the radar wavelength. MST radars transmit three beams--one vertically and two off-zenith. The radar then receives echoes from refractive index variations in the scattering volume being scanned. The drawback to this technique is that it depends on upon the existence of these variations at the three transmit angles simultaneously. Since this is not always the case, MST radars must sometimes

sample a region over a long period of time. The MST radar measures the Doppler shift induced by the moving scatterers to determine winds (Balsley, 1981).

Spaced Antenna Drift (SAD) radars are incoherent systems. They also measure Doppler shifts induced by refractive index variations. The transmitting radar beam is directed vertically, and three or more spaced receiving antennas, also directed vertically, are used to observe the return echoes. The fluctuations of echo strength at the spaced antennas are recorded. In the presence of a horizontal wind, these fluctuations show relative time displacements. Horizontal winds can be computed from the time displacements (Briggs, 1980). This method does not depend on the simultaneous existence of refractive index variations, and is the technique on which the IDI is based.

Meteor radars detect the ionized trail left by a decaying meteor as it disintegrates in the upper atmosphere above 80 km. This limits how low in the atmosphere these radars can measure winds. Meteor echoes are manifested as events with very sharp increases in amplitude followed by exponential decays. The phase history is well defined for the echo lifetime, and easily yields the radial Doppler velocity of the echo. One can calculate the mean wind profile in a given altitude interval if there are three or more echoes present in the interval (Brosnahan et al., 1987).

The fact that MST radars may require long sampling times

makes them susceptible to the influence of long period wave structures (such as gravity waves), and mesoscale motions. This makes the wind profiles obtained by them questionable (Royrvik, 1983). However, comparisons of tropospheric and stratospheric winds determined by MST radars and rawinsondes show good agreement (e.g. Warnock et al., 1978 and Fukao et al., 1982). MST radar measurements of the mesosphere did not compare as well to rocketsonde data, even though there was fair correlation between the methods (Smith and Fritts, 1984). SAD radar measurements of the troposphere and stratosphere also show good agreement with rawinsonde data (Röttger and Ierkic, 1985).

Each of these methods has provided results in obtaining wind measurements for certain atmospheric regions. Figure 1 shows the various techniques used in measuring winds in the atmosphere and the altitudes from which each technique provides results (Gage and VanZandt, 1981).

A new technique has been developed using a 50 MHz radar as an Imaging Doppler Interferometer. The frequency is high enough to allow clear-air returns from the stratosphere and troposphere and can be used to measure winds in these atmospheric regions. A big advantage to this system is that it does not require the scatterers to be in a certain place at a certain time. This radar illuminates a large volume of scatterers, and can translate the return signal into

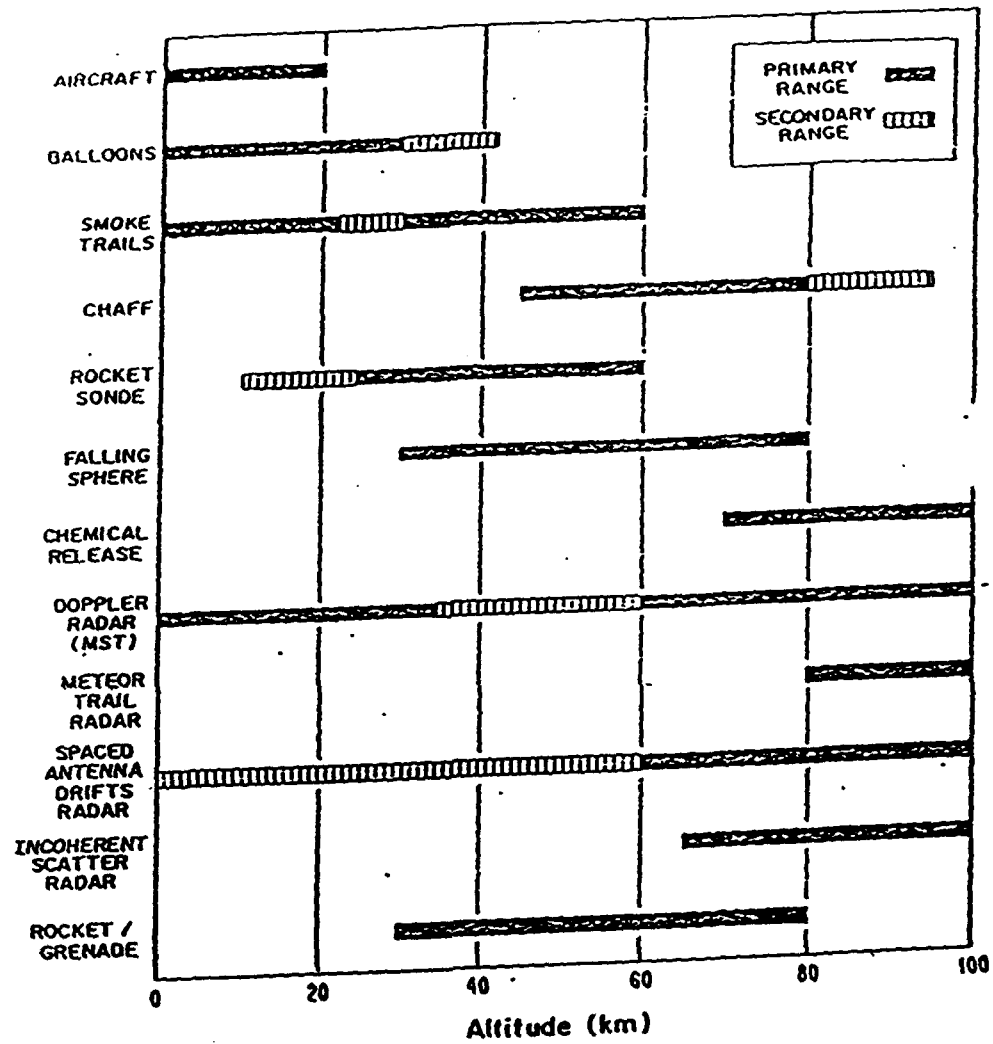


Fig. 1. Various atmospheric wind measurement techniques. (From Gage and Van Zandt, 1981.)

parameters one can use to calculate winds. Long sampling times are not required to obtain a large number of echoes, thus making the measurements more reliable. This system consists of thirty-two Yagi antennas; one array of sixteen is used as a transmitter and the other array of sixteen is used as a receiver. This method uses Fourier transforms to convert time domain data into the frequency domain. One can then use the frequency information to obtain the parameters which are used to calculate wind profiles (Adams et al., 1986).

The purposes of this thesis are as follows:

- Investigate the use of a 50 MHz Imaging Doppler Interferometer (IDI) radar to measure tropospheric winds.
- Determine the best combination for weighting and/or rejecting scattering points.
- Plot the resulting wind profiles with height and compare them with data from the Denver rawinsonde runs, the ST radar located near Platteville, CO, and the rawinsonde runs made concurrently at the radar site. I will also investigate any discrepancies between the results obtained by IDI and the other methods.
- If the results are inconclusive, I will report such a finding, and suggest further research into the IDI technique.

CHAPTER II

LITERATURE REVIEW

Probing of the atmosphere by radar depends on the scattering and reflection from spatial refractive index variations at scales of one-half the radar wavelength (Gage and Balsley, 1980). Depending on the altitude under consideration, these variations can correspond to changes in pressure, temperature, humidity, and electron density. These changes are what causes a radar signal to be scattered or reflected (Röttger, 1984). In the troposphere, electron density can be neglected, and in the upper troposphere, humidity is small enough to be negligible (Gage et al., 1981). These changes in the refractive index can best be illustrated by the following equation (Gage and Balsley, 1980):

$$n - 1 = (3.73 \times 10^{-1}e)/T^2 + (7.76 \times 10^{-6}P)/T - N_e/2N_c \quad (1)$$

where n is the refractive index, P is the atmospheric pressure in millibars, e is the partial pressure of water vapor in millibars, T is the absolute temperature in °K, N_e is the electron number density in m^{-3} , N_c is the critical plasma density in m^{-3} for the radar frequency, where $N_c = 1.24 \times 10^{-2}f^2$ and f is the radar frequency in Hz.

Doppler radar works in the following manner: when a pulse of electromagnetic radiation impinges on a target, it forces molecular vibrations in synchronism with the

time-changing electric and magnetic fields. If the target is stationary, its molecules will vibrate at the frequency of the radiation field. If the target is moving toward the transmitter at a velocity v , its vibrational frequency is higher by v/λ , (where λ is wavelength) because the target molecules experience more rapid fluctuations of electric and magnetic force due to the target experiencing more frequent strikes by the radar pulse when it's moving toward the radar (Battan, 1973). This is the Doppler effect. The vibrating molecules in turn generate electromagnetic fields, which then radiate outward from the target. For a monostatic radar where the transmitter and receiver are collocated, the frequency of the scattered radiation is Doppler-shifted; its Doppler frequency is given by $f_d = -2v_R/\lambda$, where v_R is the radial (line-of-sight) component of the velocity, positive being away from the radar. Similar reasoning applies for a target moving away from the transmitter due to the Doppler effect (Doviak and Zrnic, 1984).

Radar techniques have proven to be a very powerful tool for studying the earth's atmosphere. A technique that uses the scattering property of water/ice particles and/or the fluctuations of the index of refraction in clear air have been used to study the mesosphere and stratosphere (Woodman and Guillen, 1974). The echoes obtained from these regions come from backscattering produced by fluctuations of the atmospheric dielectric constant. Analysis of the returned

signals yields information on the dynamics of the large-scale motion as well information on the degree of turbulence (Woodman and Guillen, 1974).

The dielectric properties and, therefore, the corresponding fluctuations, are produced by different phenomena within the troposphere, stratosphere and the mesosphere. In the troposphere and stratosphere, the dielectric properties are determined by the density (i.e., by its temperature at a given pressure), while in the mesosphere these properties are determined by the number of free electrons. However, the results obtained by radar probing are independent of the mechanisms responsible for the fluctuations. If a dielectric medium is illuminated by an electromagnetic wave, the wave propagates according to the refractive and attenuating properties of the medium. In any dielectric, no matter how transparent, a fraction of the power carried in the primary wave is scattered in all directions. Fluctuations in a medium are a random process in space and time (Woodman and Guillen, 1974).

Early experiments postulated that clear air turbulence in the troposphere was responsible for the enhancement of dielectric fluctuations. Turbulence in a region with a temperature inversion is very efficient in producing fluctuations in temperature, and hence in the index of refraction. The vertical gradient of the index of refraction is given by (Woodman and Guillen, 1974):

$$dN/dz = -79 \times 10^{-6} p/T^2 \times (dT/dz + \gamma_a) \quad (2)$$

where p is the pressure in millibars, T is the absolute temperature, and γ_a is the adiabatic lapse rate in $^{\circ}\text{K}/\text{m}$. Under most circumstances, the scattering is due to atmospheric refractive index variations arising from locally homogeneous, isotropic turbulence. In the lower troposphere, these variations can also be caused by regular variations of both temperature and humidity, and are isotropic in nature (Röttger and Liu, 1978). Fresnel reflection is also responsible for producing atmospheric returns. These are caused by sharp coherent gradients in the atmospheric refractive index that extend horizontally and are produced by stratified clear air refractivity structures. These structures are usually found in the upper troposphere and the stratosphere (Balsley and Gage, 1981). Anisotropic turbulence may also play a part in the reflection of radar signals (Röttger et al., 1981).

Pertinent scale sizes of the turbulence structures which radar can detect are those corresponding to one-half the transmitted wavelength. Turbulent flow energy is transferred according to the Kolmogorov hypothesis, which says that energy enters the turbulence spectrum at large wavelengths and is transferred to smaller wavelengths until it's dissipated. This is called energy cascade (Vinnichenko et al., 1980). So, the largest scale sizes correspond to the region where turbulence is generated due to mean flow

instability. This is the energy-containing subrange. Wavelengths are on the order of several kilometers (Panofsky and Dutton, 1984). The buoyancy subrange follows, which is a sink for turbulent energy. It has a characteristic scale size of several hundred meters to one kilometer (Vinnichenko et al., 1980). Since these scales are larger than the wavelength of VHF radars, they do not contribute to the scattering/reflection process (Röttger, 1984). Energy from the energy-containing and buoyancy subranges is transmitted through the inertial subrange. Here, there is no gain or loss of energy. Wavelengths are on the order of several to tens of meters (Panofsky and Dutton, 1984). It's in the inertial subrange where VHF radar echoes are received (Röttger, 1984). The short wavelength limit of the inertial subrange is determined by viscous damping and is given by the Kolmogorov microscale λ_k :

$$\lambda_k = 2\pi(\nu^3/\epsilon)^{1/4} \quad (3)$$

where ϵ is the eddy dissipation rate of turbulence and ν is kinematic viscosity (Balsley, 1978). Scale sizes less than the microscale comprise the viscous subrange, where energy is transferred from the inertial subrange. This energy is converted into heat due to viscosity (Vinnichenko et al., 1980). Wavelengths in this subrange are on the order of 1 cm in the troposphere, and on the order of 1 m in the mesosphere. Wavelengths smaller than the microscale are strongly damped, so that the microscale essentially

determines the upper frequency limit for a radar system designed to investigate a specific atmospheric region (Balsley, 1978). However, the microscale increases with height, since it is inversely proportional to the density. Therefore, the wavelength of the turbulence structures in the inertial subrange increases with height. This is why MF radars can detect echoes in the mesosphere (Röttger, 1984).

The return signal strength in a region decreases with increasing height up to about 50 km, then begins to increase. Below 50 km, the decrease with height is primarily due to the decreasing atmospheric density and the increased stability; above 50 km, the scattering is due partly to the increase with height of the ambient ionization near the bottom of the ionosphere and partly due to enhanced neutral turbulence within the mesosphere due to increased viscous effects (Balsley, 1978). To sum it all up, since scattering typically derives from turbulence with scale sizes equal to one-half the transmitted wavelength, it's necessary to have turbulent structure of this dimension present in the scattering volume in order to obtain an echo (Balsley, 1981).

Clear air radars normally require MF-UHF (300 kHz-3 GHz) transmission frequencies, peak power of a few megawatts, and antenna apertures of hundreds or thousands of square meters. The systems must be frequency coherent (capable of determining the phase of the incoming signal relative to the transmitted pulse) in order to measure the Doppler

characteristics of the echo. One must assume that the scattering volume is completely filled with scatterers, and that the medium is homogeneous and isotropic. This assumption holds well in the troposphere and mesosphere, where homogeneous, isotropic turbulence plays a major role in scattering radar pulses. In the stratosphere, however, the stability and horizontal stratification of refractive index gradients cause the returns to be specular. In either case, there must be a way for the system to pick out real returns from noise. There are various ways in which to detect a signal from the atmosphere in the presence of noise. Figure 2 shows an example of this. The returned signal is denoted by the enhanced peak at $S_r(\Delta f) + S_N(\Delta f)$, where S_r and S_N are the power spectral densities of the signal and noise, respectively. The noise power spectral density in the absence of a signal is denoted by $S_N(\Delta f)$, and the mean value of the noise is indicated by the horizontal line \bar{S}_N . The noise fluctuation level $\overline{\Delta S}_N$ is also shown. The $\pm \Delta F$ limits are determined by the transmitted pulse rate and the number of coherent integrations, which involves the summing of a number of samples obtained from the echoing volume after sequential transmitter pulses and prior to performing a spectral analysis (Balsley, 1978).

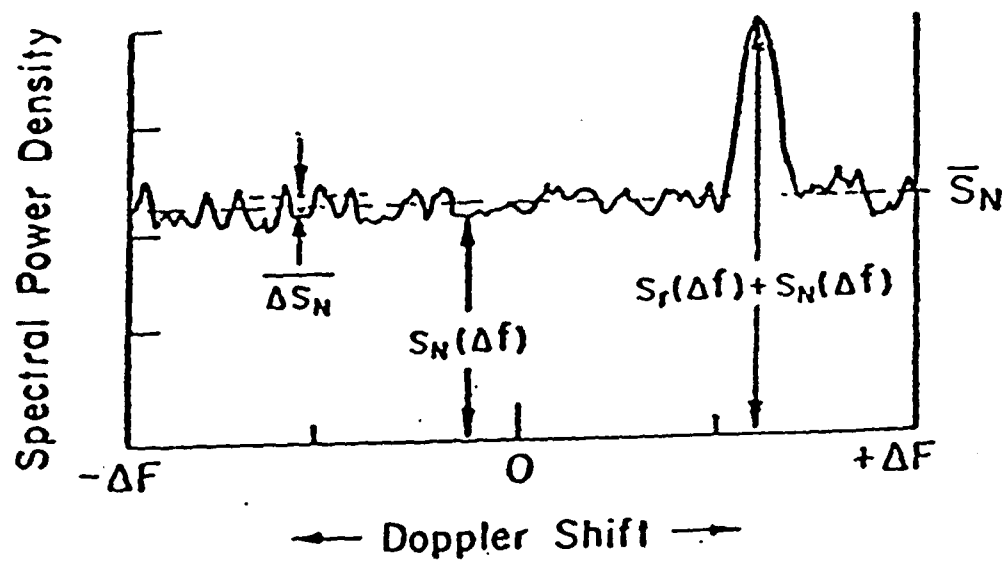


Fig. 2. Plot of spectral power density vs. Doppler shift. (From Balsley, 1978.)

To determine the vector wind at a given height, at least three Doppler measurements, each in a different direction, are required. Normally, one beam is directed to the north, 5° - 15° off-zenith, one is directed to the east, also 5° - 15° off-zenith, and one is directed vertically (Röttger, 1984). Sometimes the vertical beam is omitted on the assumption that vertical velocities may be negligible; this will provide a 2-dimensional horizontal velocity (Balsley, 1981). The two or three regions from which Doppler returns are received are separated from each other in space and sometimes also in time (Waterman et al., 1985). Recently, it was discovered that there seems to exist short period fluctuations with spatial scales less than the distance between the beam positions. These fluctuations can deteriorate wind velocity estimations. Further error would also be caused by the wind nonuniformity within the range volume which is determined by antenna aperture, transmitted pulse width, and range gate sampling (Fukao et al., 1988). The measured velocity is assumed to be an average of wind velocity within the range volume, where radio wave scattering occurs. The average does not reflect the mean wind velocity at a specific height, but is weighted by turbulence intensity (Fukao et al., 1988). Wind estimation error is then caused by the finiteness of the range volume, called the finite range volume effect (Fukao et al., 1988). This effect can produce false vertical wind shears of the horizontal velocity.

Fresnel reflection from a stably stratified atmosphere is considered as one mechanism which causes signal power decreases with increased zenith angle. This is known as aspect sensitivity (Röttger, 1984). Another mechanism involves diffuse reflection from a rough boundary between laminar and turbulent regions. One final mechanism involves the incoherent addition of reflected signals from many layers filling the volume illuminated by the radar beam (Fresnel scattering) (Gage et al., 1981; Tsuda et al., 1986).

It has been shown that the aspect sensitivity of a reflecting region increases with increasing stability (Tsuda et al., 1986). This can account for the high aspect sensitivity (specularity) noted in the stratosphere. This means that the stratosphere is filled with aspect sensitive echoes. Isotropic echoes independent of zenith angle are detected only in the troposphere. Röttger et al. (1981) determined that the angular dependence for aspect sensitive upper tropospheric and stratospheric scatterers was about 1.5-2.5 dB/degree. The stratospheric echoes with large aspect sensitivity cannot be attributed to the contribution from a single isolated reflecting surface caused by an abrupt vertical change in the refractive index, but to contributions from many reflecting layers that fill the whole stratosphere (Tsuda et al., 1986). Therefore, measurements at large zenith angles should be avoided in order to minimize errors in the horizontal wind velocities (Tsuda et al., 1986).

The radar interferometer exploits the Doppler information inherent in coherent spaced antenna measurements. Cross spectral analysis of the signals received at separate antennas can be used to locate and track irregularities while Doppler sorting can be used to discriminate against multiple targets, provided they have different radial velocities (Vincent, 1984).

The interferometer technique allows one to measure simultaneously the angular spectrum of the returns. It gives useful information on wave and turbulence structure, and improves the vertical velocity measurements (Röttger and Ierkic, 1985). The technique works only for small, localized scatterers or reflectors, and not for horizontally stratified clear air refractivity structures.

To get a value of the vertical velocity, one must know the inclination of the reflecting structures. The interferometer technique allows one to obtain the most accurate inclination measurements as well as the most accurate aspect sensitivity measurements (Röttger and Ierkic, 1985). The average inclination of the reflecting structures can give an estimate of the inclination of isentropic surfaces (Röttger, 1984). Large scale vertical motion is a consequence of nearly horizontal motion on isentropic surfaces, since parcels of air in adiabatic motion conserve potential temperature (Gage, 1983). If one can measure the motion along an isentropic surface, then the velocity vector

can be broken down into vertical and horizontal components. If this 3-dimensional wind vector is denoted by \mathbf{V}_M , then, $|\mathbf{V}_M| = (V_H^2 + w^2)^{1/2}$, where V_H is the horizontal velocity component and w is the vertical velocity component. The horizontal velocity can be broken down into zonal (u) and meridional (v) components, or, $V_H = (u^2 + v^2)^{1/2}$. Once the horizontal and vertical components are known, one can compute the baroclinicity δ by the simple trigonometric relation $\delta = \tan^{-1} (w/V_H)$. Baroclinicity is used by meteorologists to determine baroclinic instability, which effects synoptic scale disturbances that travel along the jet stream and develop into weather-producing systems (Holton, 1972). Radar measurements of baroclinicity could be used by numerical weather prediction models as an initial condition of the atmosphere. Radar interferometry provides the best measurement of vertical velocity, and could therefore be used to determine baroclinicity (Ierkic and Röttger, 1984). The vertical velocity spectra measured are due to waves, but the horizontal velocity spectra have been attributed to both quasi-two-dimensional turbulence and to the spectrum of buoyancy waves (Gage and Nastrom, 1984).

Imaging Doppler Interferometry

The technique used to analyze the data presented herein involve the principles of imaging Doppler interferometry. A 50 MHz radar operating as an Imaging Doppler Interferometer (IDI) was used, and the general concepts of interferometry

are borrowed from optics. The IDI depends on atmospheric motions to Doppler-shift the individual scatterers so that they can be separated later by performing a Fourier transform.

Radar interferometry involves making use of the phase difference between signals received at two or more spatial locations. At radio frequencies used to measure atmospheric properties, one can measure the phases of the received voltages on two or more antennas simultaneously. High-speed processing then allows one to make conventional radar measurements.

The IDI separates multiple targets by first transforming the data from time domain to frequency domain, then using the differences in Doppler phase spectra to locate the individual targets. The time series of complex voltages from each antenna are Fourier transformed, and then individual spectral features are spatially located from the phase difference between antennas. The complex Fourier transform returns both an amplitude and phase at each Doppler frequency.

Figure 3 illustrates how a single target, moving at a horizontal velocity V_H , is measured. The location and velocity of the target can be measured by Fourier-transforming the time series of the two complex voltages to get two power and phase spectra. Figure 4 is an example of the power and phase spectra for the moving target in Figure 3. Both power spectra identify the same Doppler frequency f , which can be used to obtain the the radial velocity V_R :

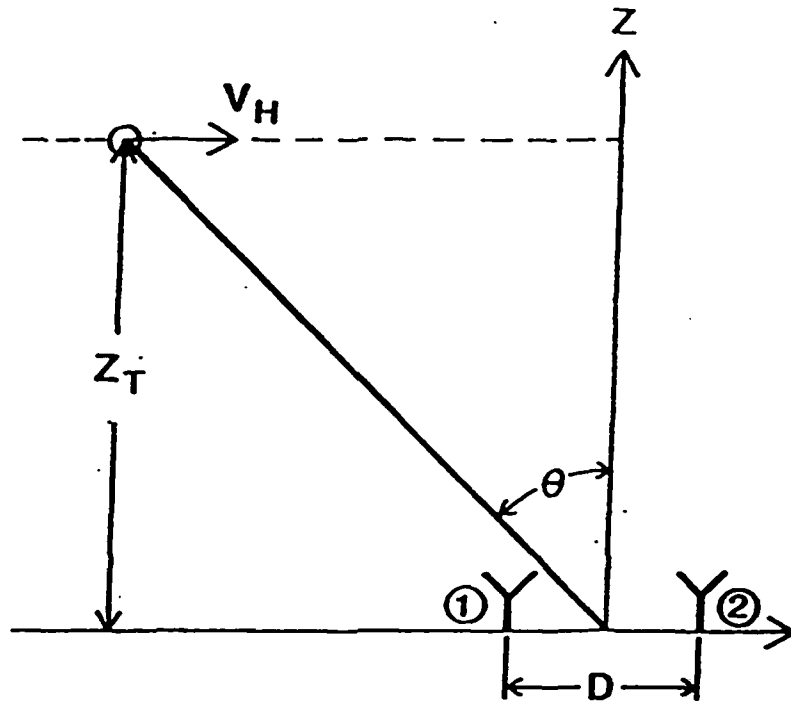


Fig. 3. Geometry for single horizontally moving target being viewed by a two-antenna interferometer. (From Adams et al., 1985.)

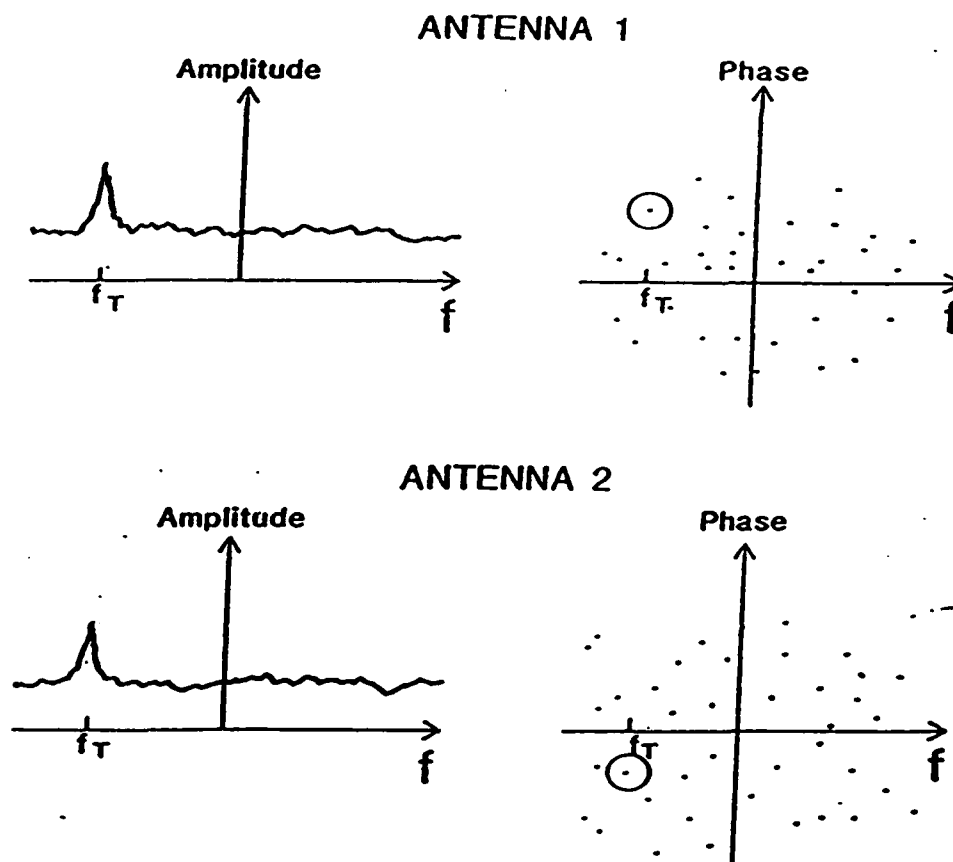


Fig. 4. Complex Fourier spectra for the two antennas in Figure 3, showing the signature of a single moving target. (From Adams, et al., 1985.)

$$V_R = fc/2F = V_R \sin\theta \quad (4)$$

where f is the Doppler frequency, F is the radar frequency, and c is the speed of light. The difference in phase angles can be used to calculate the zenith angle:

$$\theta = \sin^{-1} (\phi\lambda/2\pi l) \quad (5)$$

where l is the spacing between the two antennas, λ is the radar wavelength, and ϕ is the phase (Adams et al., 1986).

The 50 MHz IDI, however, uses thirty-two antennas, so a slightly different approach is used. Radar returns are received on eight independent antennas. Each antenna's data are separately Fourier-transformed, and the resulting complex Fourier spectra at each range gate are examined for Doppler bins whose sources can be located by spatial interferometry. Real sources are identified by requiring agreement among the independent antenna pairs on the two-dimensional angular location of each source.

One can then determine a set of characteristics that will define each individual scattering point; these characteristics are the scattering point parameters (SPPs) and consist of:

- z : the altitude at which the echo is located;
- V_R : the echo radial velocity;
- θ_{EW} : the echo-location angle in the E-W plane;
- θ_{NS} : the echo-location angle in the N-S plane;
- V_{EW} : the average voltage on the E-W antenna;
- V_{NS} : the average voltage on the N-S antenna;

ϕ_{EW} : the phase on the E-W antenna, relative to the center of the array;

ϕ_{NS} : the phase on the N-S antenna, relative to the center of the array.

Now we have defined a three-dimensional coordinate system, which one can transform to a Cartesian system (X is east, Y is north, and Z is vertical). The scattering point parameters are sorted by altitude. One can now calculate the mean apparent motion of each scattering point. The radial velocity of each scatterer can be calculated from equation 4 as:

$$V_{Rj} = cf_j/2F \quad (6)$$

where $j = 1, 2, 3, \dots, J$, where J is the number of scattering points. One can also write the vector radial velocity as:

$$\mathbf{V}_{Rj} = V_{Rj} \mathbf{l}_{Rj} \quad (7)$$

where \mathbf{l}_{Rj} is a unit vector in the radial direction passing through the j th scattering point, given by:

$$\mathbf{l}_{Rj} = l_j \mathbf{l}_x + m_j \mathbf{l}_y + n_j \mathbf{l}_z \quad (8)$$

where l_j , m_j , and n_j are the direction cosines of the j th scattering point, given by:

$$l = \sin \theta_{EW} \quad (9)$$

$$m = \sin \theta_{NS} \quad (10)$$

$$n = (1 - l^2 - m^2)^{1/2} \quad (11)$$

Then, the mean apparent motion vector can be denoted as:

$$\mathbf{V}_m = u \mathbf{l}_x + v \mathbf{l}_y + w \mathbf{l}_z \quad (12)$$

Three scattering points are the minimum required to determine

the three components of motion. With these points, one can calculate a least-squares fit to the SPPs as follows: Since

$$V_{Rj} = \mathbf{V}_m \cdot \mathbf{l}_{Rj} \quad (13)$$

for all j if the rms fit is perfect, the rms error is given by:

$$\epsilon = \{1/J\Sigma[V_{Rj} - (ul_j + vm_j + wn_j)]^2\}^{1/2} \quad (14)$$

We need to choose the values of u , v , and w that minimize ϵ , or:

$$\partial\epsilon/\partial u = \partial\epsilon/\partial v = \partial\epsilon/\partial w = 0 \quad (15)$$

which then yields:

$$u\Sigma l_j^2 + v\Sigma l_j m_j + w\Sigma l_j n_j = \Sigma V_{Rj} l_j \quad (16)$$

$$u\Sigma l_j m_j + v\Sigma m_j^2 + w\Sigma m_j n_j = \Sigma V_{Rj} m_j \quad (17)$$

$$u\Sigma l_j n_j + v\Sigma m_j n_j + w\Sigma n_j^2 = \Sigma V_{Rj} n_j \quad (18)$$

These equations can then be solved simultaneously for u , v , and w , which then give the three-dimensional bulk flow for each range gate.

CHAPTER III

DATA ANALYSIS

The MENTOR 50 MHz IDI Radar

The data used for the analysis were collected by the 50 MHz MENTOR Imaging Doppler Interferometer (IDI) radar, located near LaSalle, Colorado ($40^{\circ}16'42''\text{N}$, $104^{\circ}35'55''\text{W}$). The MENTOR (Meteor Echoes; No Transmitter, Only Receivers) had originally been designed to be a passive system, receiving pulses reflected out of ST radar beams by meteor trails. A 50 kW transmitter was later added so that a stand-alone IDI radar, used to measure tropospheric and stratospheric winds, could be deployed. The MENTOR operates at frequencies between 49.8 and 49.92 MHz, with 50 kW peak-pulse-power in pulse lengths of 1.67 or 6.67 μsec . The pulse repetition rate is variable from 470 μHz to 12 kHz. One complete sounding contains 256 samples, and it takes 10 seconds to obtain one sounding.

Figure 5 shows graphically how the system is set up. Two identical arrays of 16 5-element vertically directed Yagis are used; one array is the transmitter, the other is the receiver. Both are arrayed in a four-by-four matrix with 1.05-0.7-1.05 wavelength spacing between both the row and column antennas. The transmit antennas are fed with a 16-way power splitter with equal power and phase. The resulting beam is approximately 20° wide at the 3-dB points. On the



Fig. 5. The MENTOR set-up.

receive array, the 16 signals are power-divided with 0° hybrids, and these signals are recombined with 4-way power combiners to obtain a total of 8 outputs consisting of 4 row arrays and 4 column arrays. Each antenna's pattern is fan-shaped, being 20° wide along the line of Yagis and about 50° perpendicular to the line of Yagis. The MENTOR uses a direct-conversion receiver technique. A total of 8 channels are used to amplify and detect the 8 antenna signals (Brosnahan et al., 1988).

During data collection, coherent averaging is done and is dynamically adjusted to maintain a TDA output rate of 256 samples every 10 seconds. An FFT is then done on the data to yield results in the frequency domain, from which the scattering point parameters are derived. From this point, one can then calculate wind profiles in the lower and middle atmosphere.

Tropospheric Wind Analysis

In the past, a 2.66 MHz IDI radar was used to determine mesospheric wind profiles. The MENTOR was designed to measure winds from the troposphere and stratosphere as well. It can measure winds in these regions due to its high sensitivity and its ability to gather the data needed to provide wind calculations in a relatively short time period. The MENTOR also possesses extremely fast data-processing hardware, which makes gathering the data and its conversion to scattering point parameters via an FFT routine possible.

Figure 6 is a computer block diagram of the MENTOR system setup.

In order to calculate the winds, I first developed software to make the basic calculations. I tested it in two different ways. First, I took three points at 5.1 km. One point was directly overhead (θ_{EW} and θ_{NS} both equal to zero), one was 10° off-zenith on the E-W array and the other was 10° off-zenith on the N-S array. The test wind was 30 m/s from 260° . This gave a zonal component (u) of 29.54 m/s and a meridional component (v) of 5.21 m/s. I let the vertical component (w) equal zero for this test. I then derived radial velocities for each of the three points, and used these values along with the values of θ_{EW} and θ_{NS} in the program. I obtained $z = 5.1$ km, $u = 29.6$ m/s, $v = 5.24$ m/s, $w = 0.0$ m/s, horizontal velocity = 30.06 m/s, and horizontal direction = 260° . This provided a simple check to insure the logic and correctness of the routines. I then analyzed synthetic data derived to further test this program (see Adams et al. (1985) for information relating to the generation of these data). The horizontal velocity was input to be a constant 30 m/s, with the horizontal direction vector rotating counterclockwise.

In order to analyze the synthetic data, I first calculated the rms error using the technique described in the last chapter (equation 14). After calculating the components

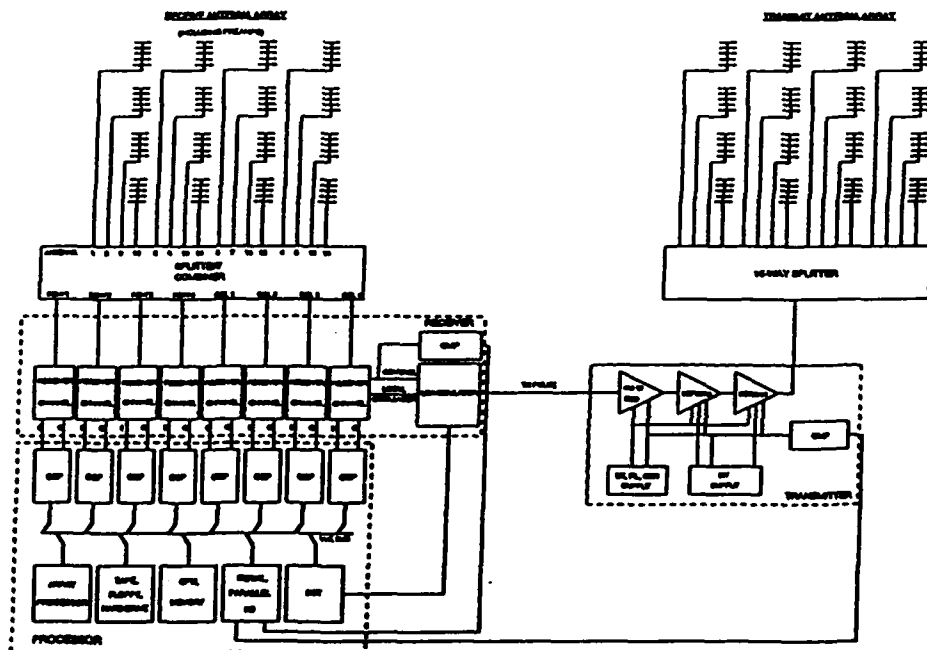


Fig. 6. MENTOR block system diagram.

and the rms error for each range gate, I then discarded those points where the individual error was greater than twice the rms error for the particular range gate and recalculated the winds. The input to the synthetic data (Figure 7) is the desired result. I varied the number of points per velocity in each profile to see if more points produced a better average. The results for 10, 15, 30, and 60 points are shown in Figures 8-11. Each profile approximates the input quite well. It appears that more points per velocity calculation provides better average results, with the curve becoming smoother with each subsequent increase in points. The largest value of V_H for 10 points was 32.5 m/s, for 60 points it was 31.8 m/s; the smallest value of V_H for 10 points was 27.2 m/s, for 60 points, it was 29.1 m/s. However, it is apparent that these differences are minor, and that using fewer points provides better altitude resolution. The ideal situation would be to use as few points as possible so that one can obtain a very dense profile.

The actual data analyzed were obtained 14 Oct 88 from 18:25 UT to 20:15 UT. These data will be compared to National Weather Service rawinsonde runs at 14 Oct/12:00 UT and 15 Oct/00:00 UT out of Denver, two rawinsonde balloons launched at the radar site to coincide with the radar data acquisition, and data from the ST radar run by NOAA/WPL near Platteville, CO. The rawinsonde launches at the radar site are extremely desirable: Denver is approximately 60 miles SW

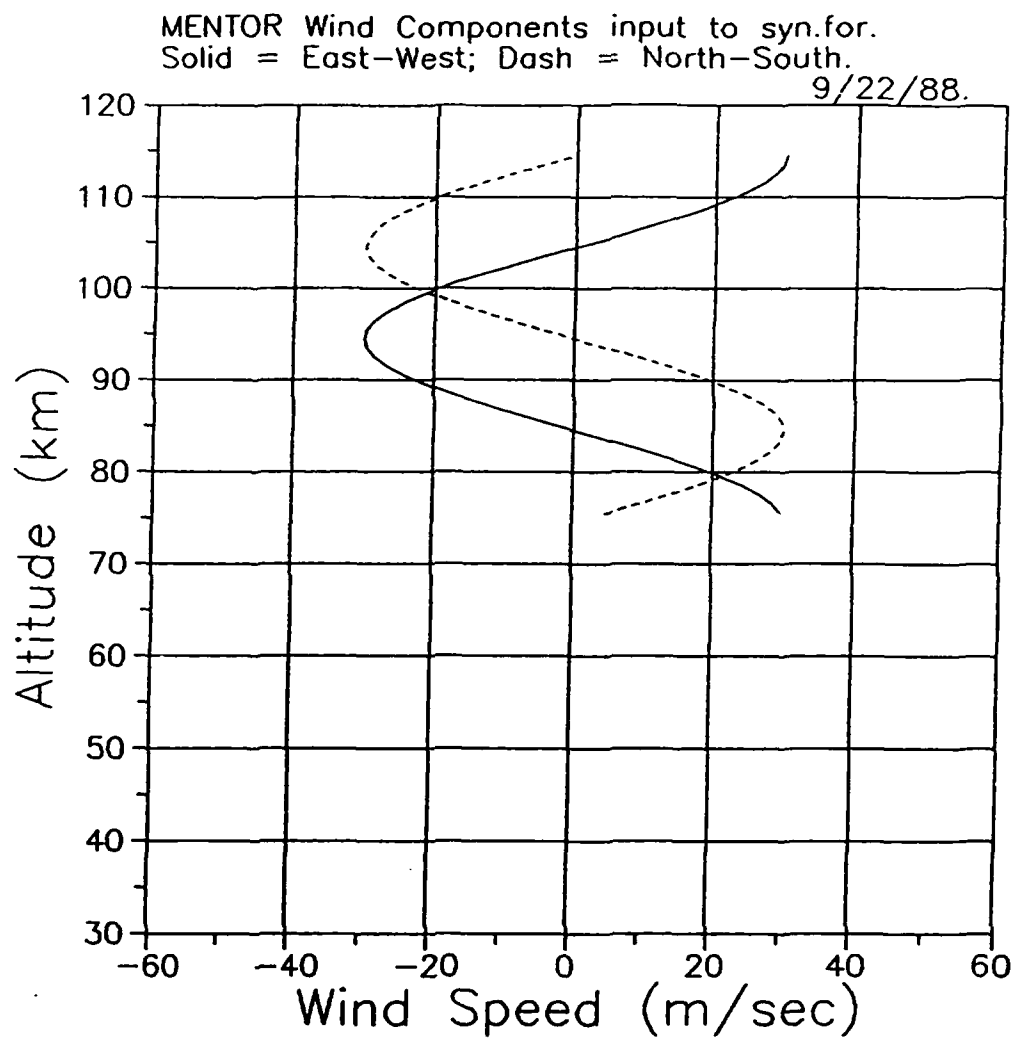


Fig. 7. Wind component input to synthetic data generator.

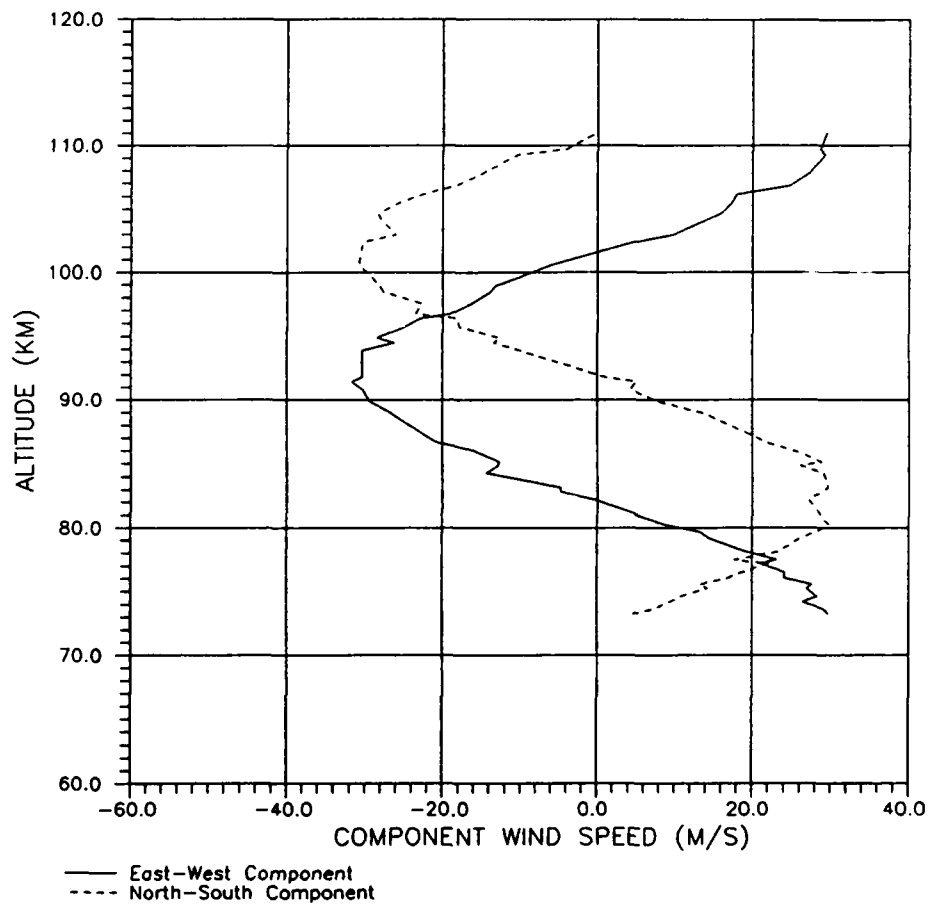


Fig. 8. Test calculations using synthetic data and 10 points per velocity.

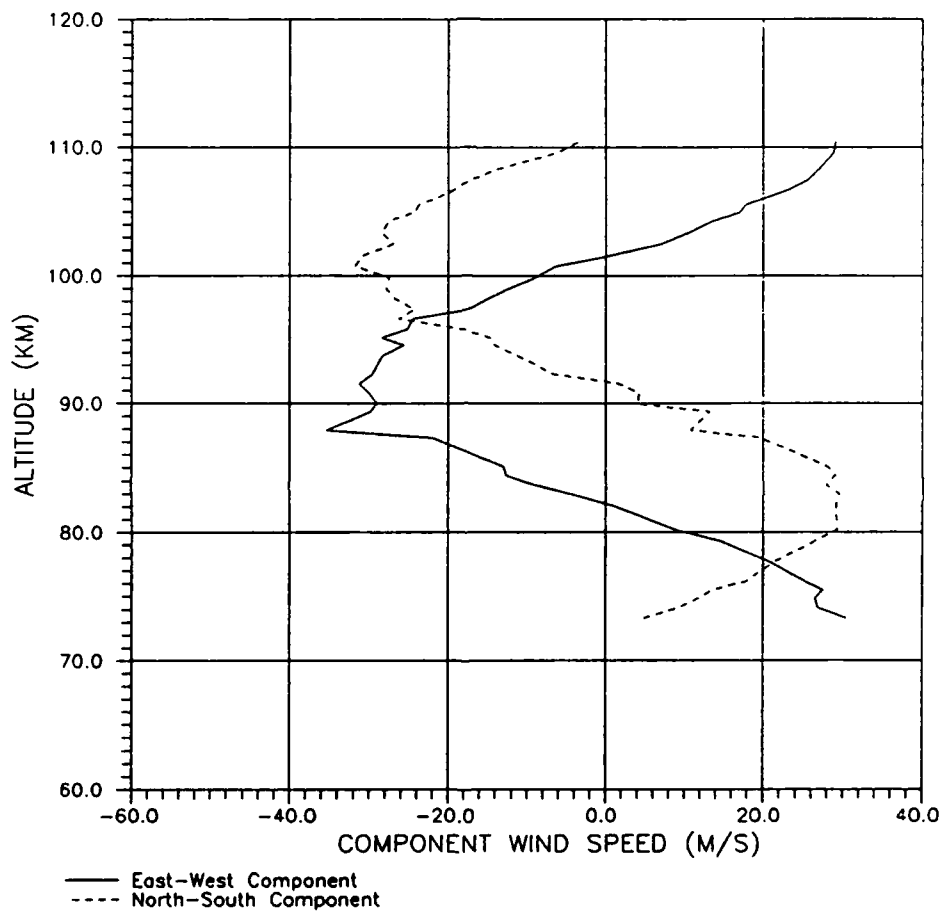


Fig. 9. Test calculations using synthetic data and 15 points per velocity.

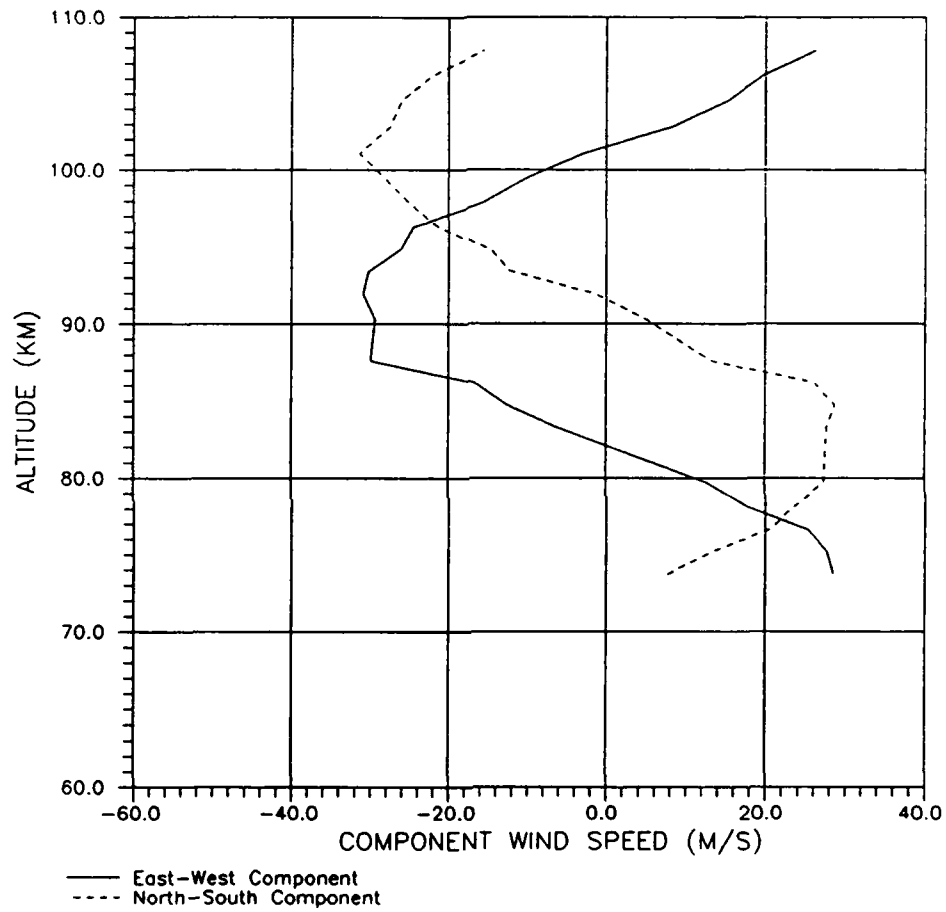


Fig. 10. Test calculations using synthetic data and 30 points per velocity.

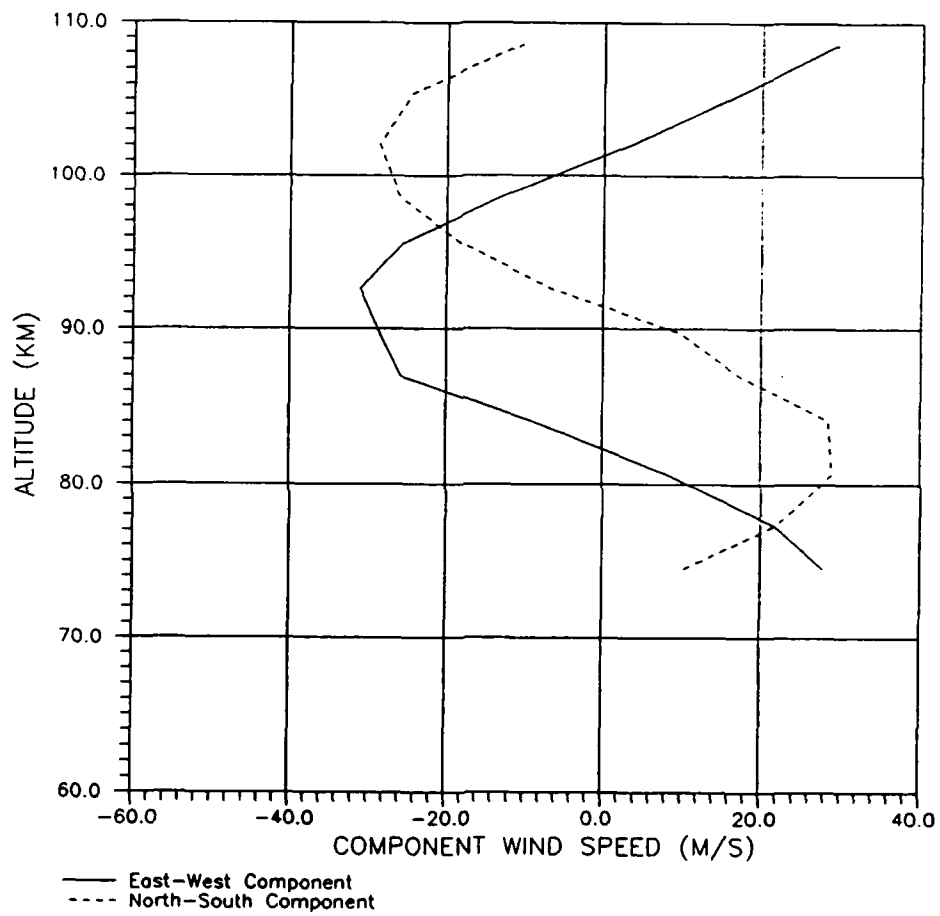


Fig. 11. Test calculations using synthetic data and 60 points per velocity.

of the radar site, in the foothills of the Rockies, and the winds measured there can be influenced more by the mountains than those at the radar site, which lies on the high plateau east of the base of the mountains. Also, winds are a dynamic feature; even 5 minutes can make a substantial difference in wind velocity. Thus any discrepancies noted between the Denver runs and the IDI could be cleared up by the data from the local rawinsonde run. A comparison between the IDI and the conventional ST radar will also prove interesting. Platteville is approximately 10 miles SW of LaSalle, and it's also on the high plains east of the foothills. There should be little difference in the mean flow over the two sites; therefore this can be considered a comparison of the two radar techniques. In comparing the IDI data with the LaSalle rawinsonde data, one must consider the fact that as the rawinsonde balloon rises, it is carried horizontally with the wind. On the average, a balloon takes one hour to reach a height of 5 km. If one uses an average horizontal wind of 5 m/sec over that altitude range, it is displaced by 43 km from its launch site. Then, the wind measured at 5 km by the IDI is overhead, while that measured by the balloon may now be 43 km away.

The two balloon launches at LaSalle were at 18:22 and 19:42 UT, and the Platteville ST run was at 19:00 UT. I developed software to break down the horizontal velocities from the ST and balloon observations into components; these

components will be compared to those obtained by MENTOR.

Dr. Gene Adams (Personal Communication, 1988) developed the main software program that I used to derive the tropospheric winds from MENTOR. One of the major problems one needs to resolve is determining which points received are good and eliminating any ambiguities in the reception of points. For this purpose, the antennas were set as shown in Figure 5. The two Yagis closest to each other are 0.7λ apart, while the distance between the end and middle Yagis are 1.05λ , making the total distance between the end Yagis 2.8λ . Thus, one can measure the phase at each of the four Yagis: ϕ_1 and ϕ_4 at the ends and ϕ_2 and ϕ_3 at the two in the middle. There are also four complex voltages measured, which gives three independent phase differences: $\phi_1 - \phi_2$ (1.05λ), $\phi_3 - \phi_2$ (0.7λ), and $\phi_4 - \phi_3$ (1.05λ). Each phase difference corresponds to one or more possible zenith angles through the interferometer equation:

$$\Delta\phi = -2\pi D \sin\theta \quad (19)$$

where D is the antenna spacing in wavelengths. Thus, for the two pair of Yagis 1.05λ apart, $\Delta\phi = 2.1\pi \sin\theta$, and for the pair that are 0.7λ apart, $\Delta\phi = 1.4\pi \sin\theta$. Solutions of these two equations yield several values of θ . A variable zenith angle window is then used. There are three independent measurements of the E-W zenith angle, which will spread across some range of zenith angles, and three simultaneous measurements of the N-S zenith angle and their resultant

spread. The sum of the two maximum spreads of zenith angles in each direction derived from the three independent phase differences (the 0.7λ pair and the two 1.05λ pair) must be less than the specified zenith angle window for one of the possible $\pm 2\pi$ permutations. The basic design of the window is as follows: there are several zenith angles in both the E-W and N-S directions. For the first time through the window routine (the E-W values), the maximum allowed zenith angle spread is the user-defined zenith angle window. The second time through the routine (the N-S values), the maximum allowed spread is the user-defined window minus the actual E-W value. Then, equation 19 gives the relationship between the antenna-to-antenna phase difference and zenith angle. For spacings larger than 0.5λ , two or more zenith angles are possible solutions for a given phase difference. For the 1.05λ and the 0.7λ spacings, three solutions exist. One determines the maximum and minimum zenith angles for each direction, and calculates the spread, or:

$$\theta_{\text{spread}} = \theta_{\text{max}} - \theta_{\text{min}} \quad (20)$$

If the smallest spread is greater than the zenith angle window, the point is rejected. If it's less, then the actual zenith angle has been located. The spreads calculated on both the E-W and N-S arrays are written as scattering point parameters. A consensus angle is then defined as the middle of the calculated window, or:

$$\theta_{\text{consensus}} = (\theta_{\text{max}} - \theta_{\text{min}})/2 \quad (21)$$

A second check is then done by coherently averaging the voltages from each pair of antennas located 1.05λ apart, then calculating the phase difference between them. This will generate five values of θ from a single phase difference. The values of θ obtained by both methods are then compared; only one of the solutions obtained by coherent averaging will be within the window centered on the consensus zenith angle. This is the final zenith angle, which improves the accuracy of the calculated consensus value by a factor of $(N_i)^{1/2} * N_c * D$, where N_i is the number of incoherent averages, N_c is the number of coherent averages, and D is the antenna spacing in wavelengths. If there are no values that lie within the window centered on the consensus angle, then the point is rejected. Setting the window to a larger value obviously allows more noise into the system, but also lets more true points in as well. Smaller values decrease both noise and true points. One must use trial-and-error methods to determine which value of the window is optimum, and also make use of filters to weed out system-generated points and any others that may contaminate the data. For this analysis, I found that a zenith angle window of $24'$ worked best.

I used a linear polarization filter in conjunction with doing an FFT on the time domain data. This is done to match the transmit polarization.

After the time-domain data were transformed to the SPP format, I merged consecutive strings of 10-second soundings

together to create one long sounding of various lengths. I did this so that I could plot the various parameters against each other to see if there were any patterns evident in the distribution. I also wanted to have various sounding lengths available when I did the wind profiling; this way I could determine what the optimum sounding length should be. The sounding lengths were 2, 3, 4, 6, 8, and 10 minutes. Initial review of 10 minutes of data taken from 18:25:10 to 18:35:10 UT on 14 Oct 88 showed that the radial velocities obtained by MENTOR were contaminated with noise. Figure 12 shows a scatter plot of radial velocity versus radial zenith angle, showing radial velocities much greater than zero for angles near zenith. This would translate roughly into high vertical velocities, on the order of $\pm 30-40$ m/s, since the radial velocity near zenith is mostly composed of vertical velocity. Such high vertical velocities are unrealistic, and would correspond to horizontal velocities near zero for points near zenith. In order to filter out these points, six 10-second soundings were coherently averaged, and the results plotted. A least-squares polynomial was then fit to these data. This filtered out the high radial velocities close to zenith while keeping the other points. The coherent average was done in order to enhance the pattern, especially near zenith. The one-minute average cut down the number of points and made it easier to determine a pattern and to fit the curve. The algorithm was then used as a filter for the merged data

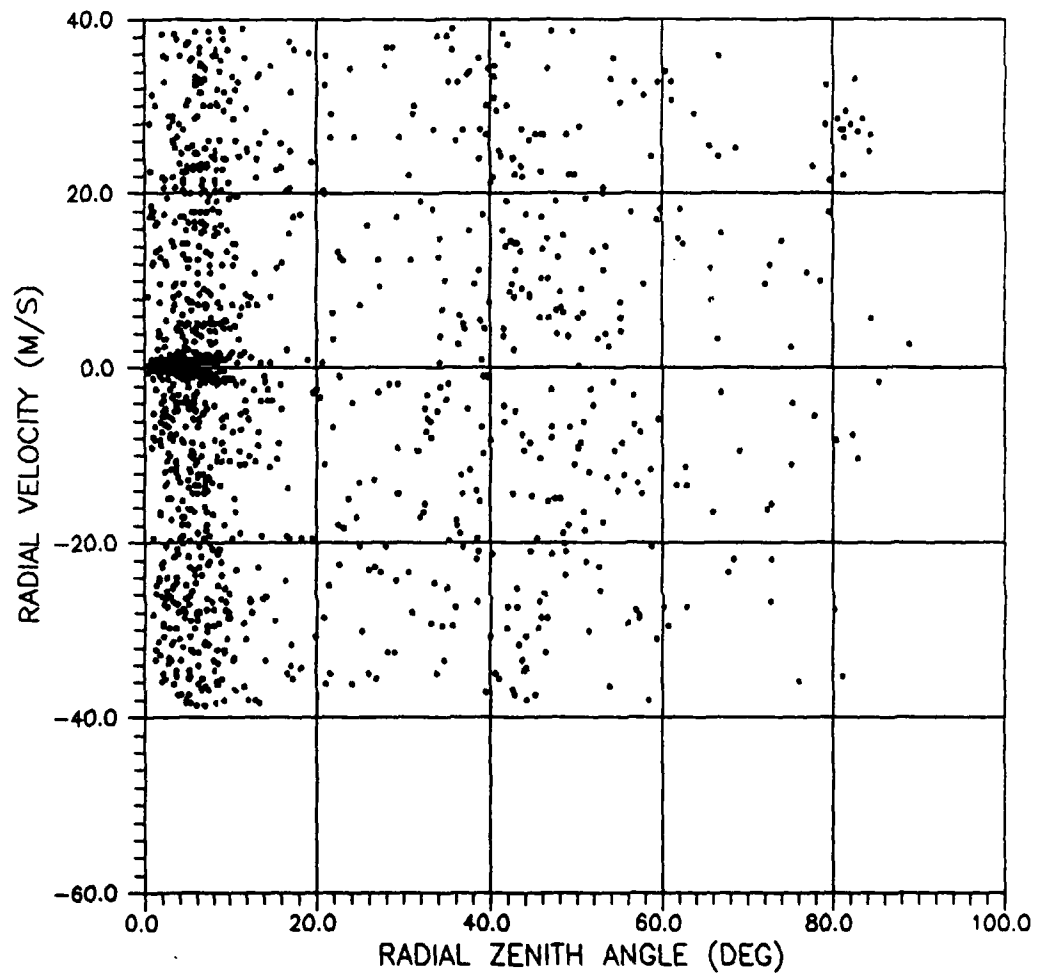


Fig. 12. Scatter plot of radial zenith angle vs. radial velocity from 10 minutes of MENTOR data.

files.

Generally, points that are received near zenith give a good representation of vertical velocities, while points further off-zenith will provide good results for horizontal velocities. Knowing this, I separated the merged data into bins; the first one for points that lie within $\pm 2^\circ$ of zenith, another for points between $\pm 2^\circ$ and $\pm 10^\circ$ off-zenith, and another for points between $\pm 10^\circ$ and $\pm 25^\circ$ off-zenith. I decided to try using only points within $\pm 2^\circ$ of zenith for vertical velocity profiles, and points further off-zenith for horizontal profiles. Interestingly, I obtained fairly good results for both vertical and horizontal velocities using the data within $\pm 2^\circ$ of zenith, while the results using points further off-zenith provided results that did not correlate at all with the results from the other techniques. Once I noted this phenomenon, I tried opening up the point-collection window to $\pm 3^\circ$, since there would be more points in that extra degree that I could use to generate more wind values in a profile. However, this only contaminated the data, and I found no agreement. I then opened up the window to $\pm 10^\circ$ using a 1° increment. The results were the same: no agreement. I then tried keeping only points within $\pm 1^\circ$ of zenith, but there were not enough points to provide more than 2 wind values in the troposphere. At first, it seemed very unusual that only those points within $\pm 2^\circ$ of zenith would provide reasonable wind profiles.

I plotted the east-west and north-south zenith angles versus altitude and the east-west and north-south returned voltages versus the east-west and north-south zenith angles, respectively (Figures 13-16). These scatter plots show what is happening: note the cluster of scattering points near zenith in Figures 13 and 14. This shows that a majority of returns are coming from near zenith. The scatter plots in Figures 15 and 16 show that the received voltages are orders of magnitude higher close to zenith. This means that all the returns from points not close to zenith are noise. This is due to the fact that the power transmitted falls off rapidly with zenith angle, so that there is effectively no signal going out past approximately $\pm 2^\circ$, and many of the returns past that are noise. Figures 17 and 18, which are plots of the east-west and north-south received voltages versus altitude, further illustrate this.

From Figures 13 and 14, one notices that there are not as many scattering points near zenith at altitudes between 4 and 10 km as there are at altitudes below 4 km and above 10 km. Then Figures 17 and 18 show that the returned voltages have peaks below 4 km and above 10 km. This can be attributed to the loss of signal power at points far enough off-zenith. This signal power fall-off is a function of the antenna frequency; the higher the frequency, the narrower the transmitted beam. One could lower the frequency and widen the beam, but at the expense of low-altitude returns. The

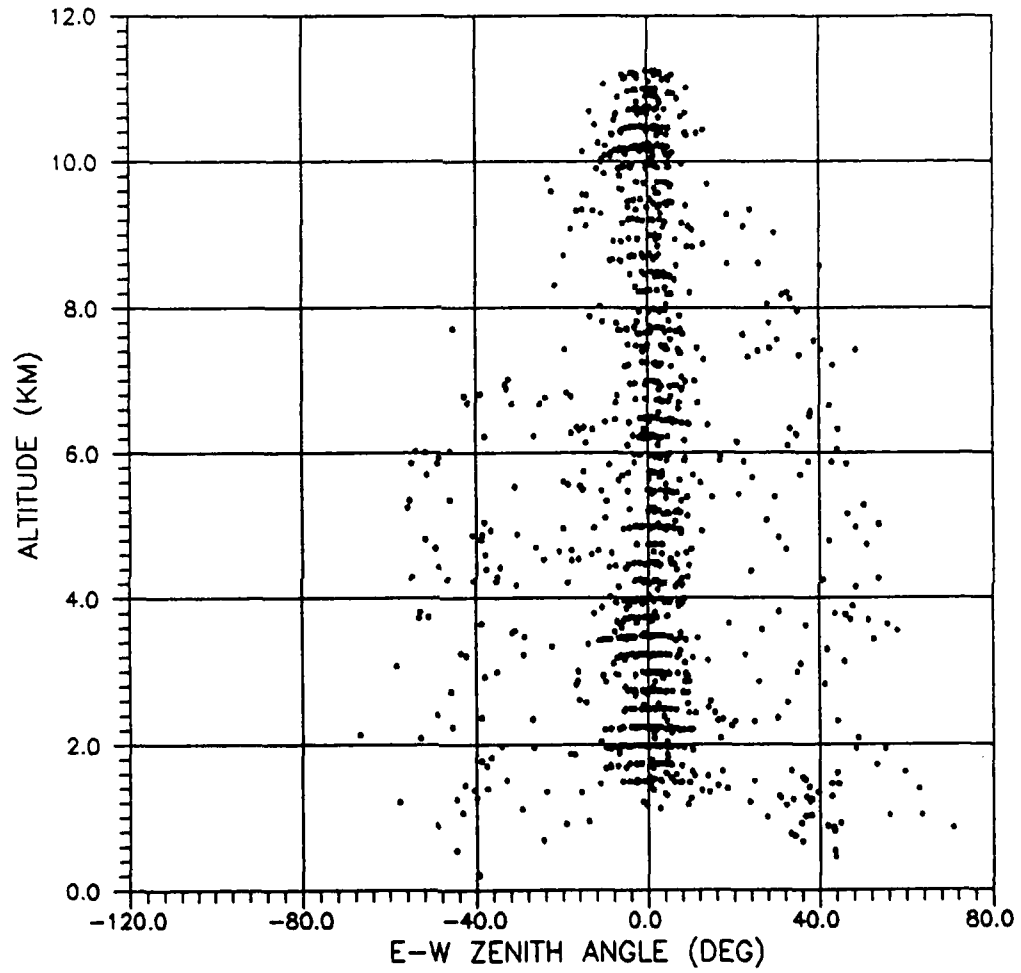


Fig. 13. Scatter plot of E-W zenith angle vs. altitude from MENTOR.

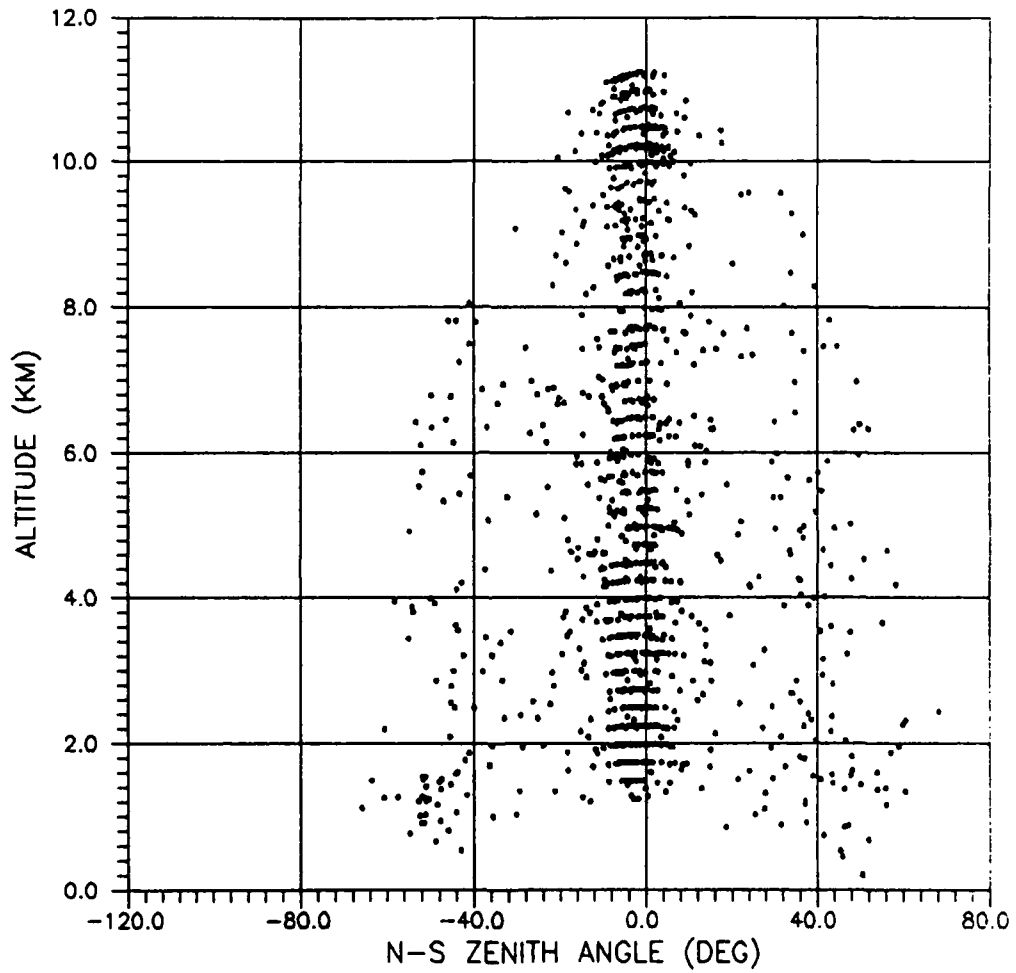


Fig. 14. Scatter plot of N-S zenith angle vs. altitude from MENTOR.

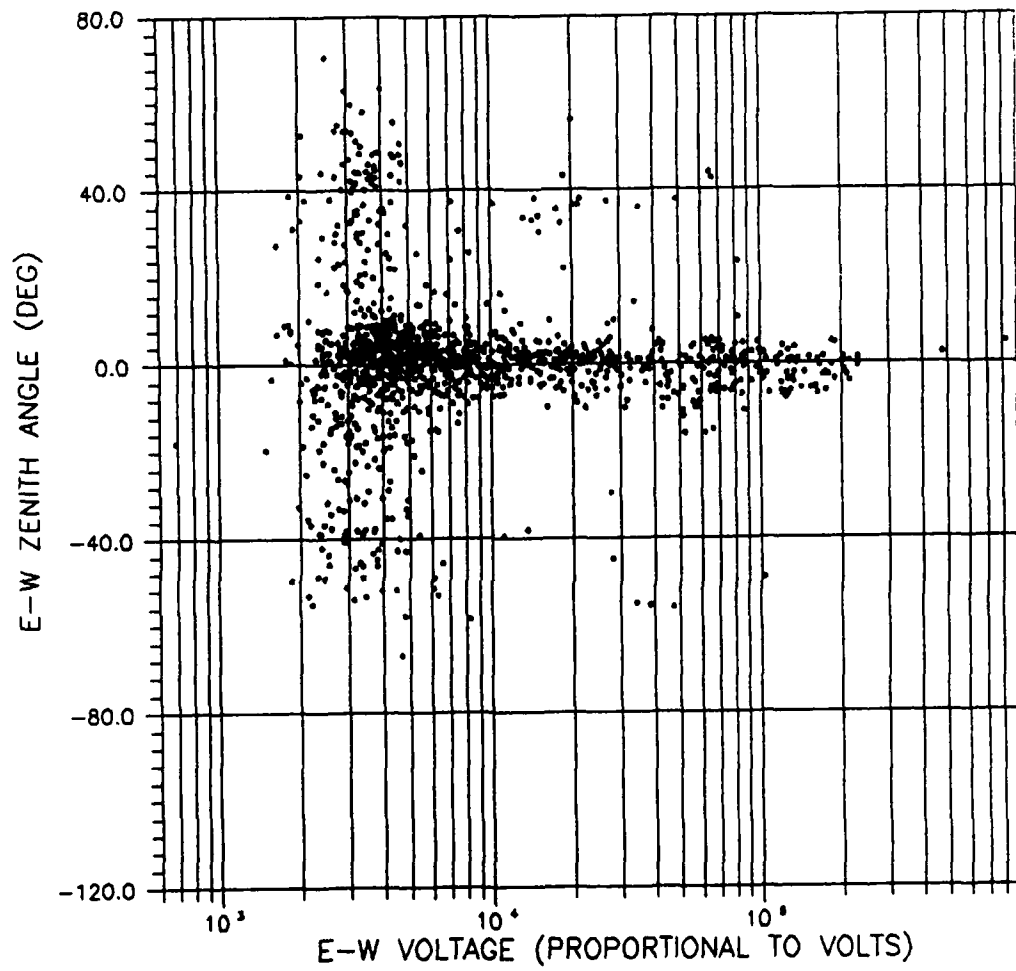


Fig. 15. Scatter plot of E-W received voltage vs. E-W zenith angle from MENTOR.

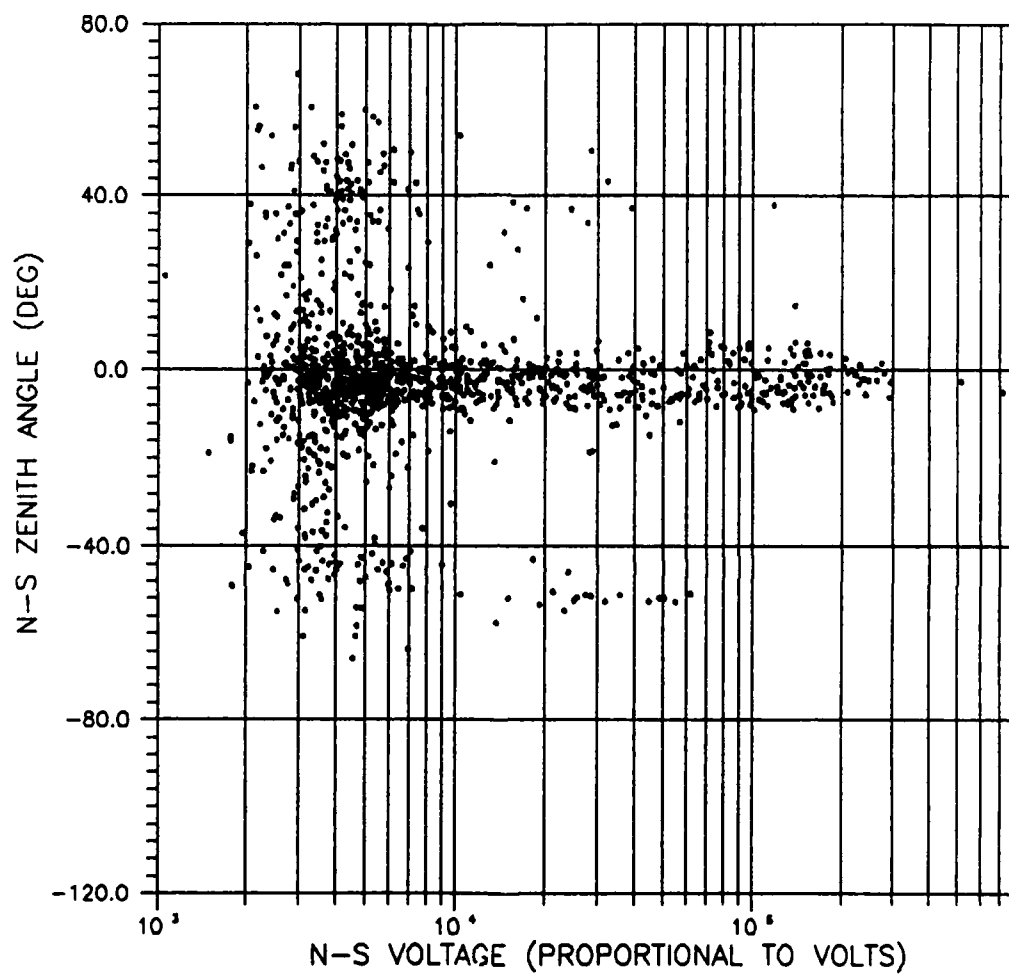


Fig. 16. Scatter plot of N-S received voltage vs. N-S zenith angle from MENTOR.

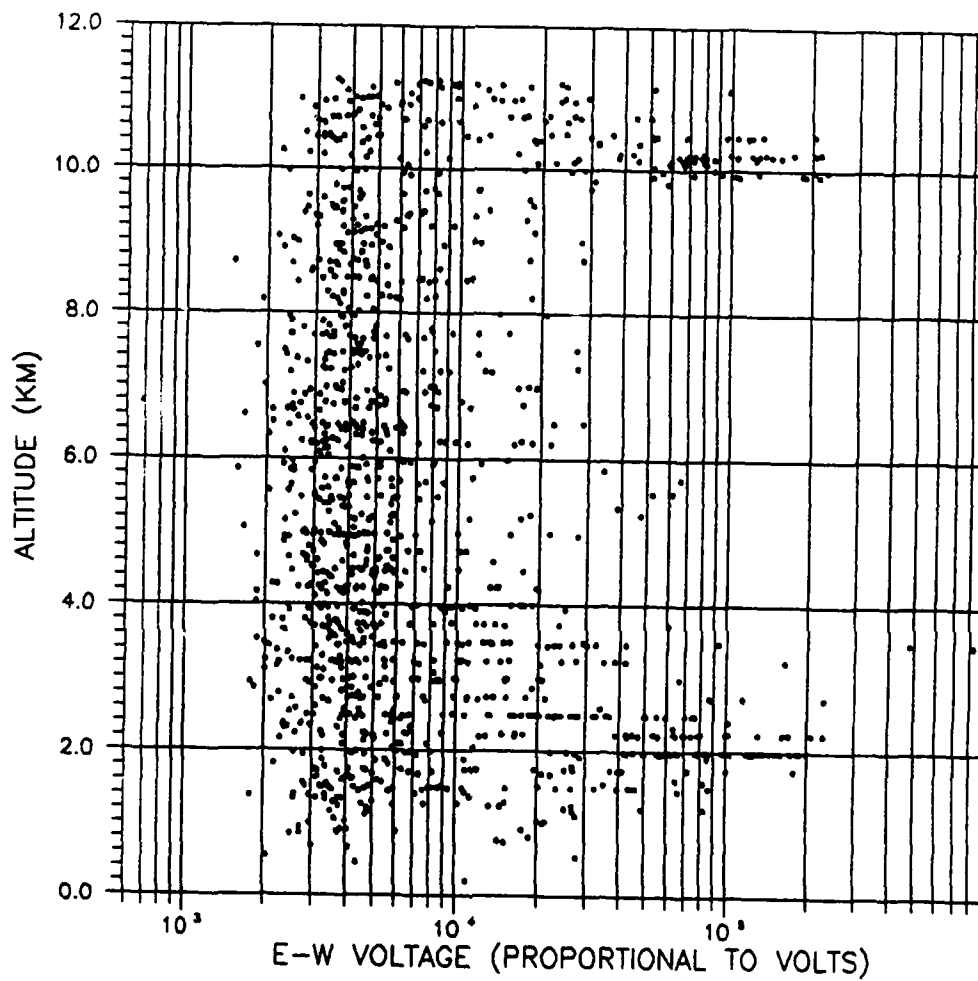


Fig. 17. Scatter plot of E-W received voltage vs. altitude from MENTOR.

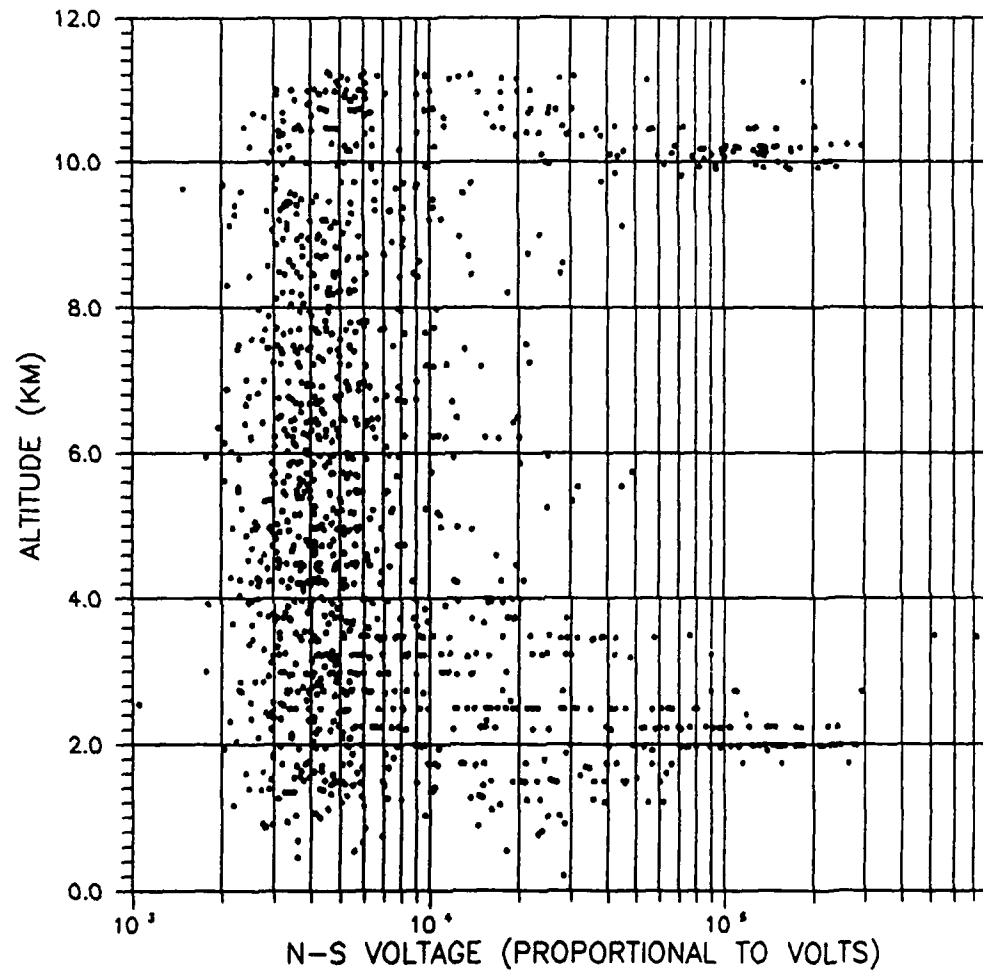


Fig. 18. Scatter plot of N-S received voltage vs. altitude from MENTOR.

occurrence of good returns only near zenith could be a property of the scatterers, independent of beamwidth. Incidentally, other experiments using radar interferometers to measure atmospheric winds found that even at small off-zenith angles, the horizontal component of the average velocity is not negligible and could be measured (Röttger and Ierkic, 1985).

After calculating multiple wind profiles and doing comparisons with the other data, I was able to determine that using a zenith angle window of 12° or 16° did not provide enough data to plot a usable wind profile, even after merging enough consecutive files to create a 10-minute sounding. Opening the window to 20° and 24° lets in more points (and noise), but the filters that are applied to the data work to effectively keep the noise out. When calculating the profiles using these data, I discovered that using fewer points allows for better altitude resolution, so more points can be plotted with height. I also noted that the results I obtained by discarding points that had an error of more than twice the rms error in the given range gate were not significantly different than those obtained by keeping all the points. Even after opening the zenith angle window to 24° , the filtering process takes its toll on the number of points left with which to calculate wind profiles. For this reason, I used 10 minutes of consecutive data to calculate the profiles presented in the next chapter. There are simply

not enough points when using soundings much shorter than that. I used two separate 10-minute soundings to calculate profiles, the first from 18:25:10 to 18:35:10 UT and the second from 18:45:10 to 18:55:10 UT. These were the only two tapes in which there were enough continuous data to complete a 10-minute sounding.

If more continuous data were available, longer soundings could be created, and profiles with better resolution could be calculated. However, this too has its drawbacks. As a scatterer approaches the radar beam from a distance, it moves through several Fourier windows as it moves across the sky and through the beam. This means that the Doppler shift changes each time the scatterer passes through a different window. The longer the sounding, the more windows the target passes through. This has an effect on the wind velocity that is calculated, and is known as velocity smearing. Unfortunately, smearing is a complex process, and no one to date has been able to determine how to "desmear" the data.

After the data analysis was completed, I found out that there was a problem with one of the antennas. Apparently, the y-component on antenna number four was always zero, which would induce errors in the echo location. Even though this is a problem, so much filtering takes place that most of the bad pints were probably removed. One could also develop a filter to eliminate all the data from antenna four before using them to calculate winds.

CHAPTER IV

RESULTS AND DISCUSSION

This chapter contains the wind profiles calculated using the MENTOR data and the technique developed to analyze them. The wind velocities calculated are not instantaneous, but time-averaged bulk flow rates. Only extremely sensitive sonic anemometers can measure instantaneous wind velocities. The MENTOR is providing the average wind velocity in a given range gate over a 10 minute period.

The data presented include plots of the horizontal velocity, its zonal and meridional components, vertical velocity, the direction from which the horizontal wind is coming, and baroclinicity. Standard meteorological notation is used in order to coincide with the data taken from the rawinsondes and the ST radar. This means that the horizontal direction of the wind, α , is given by $\alpha = \tan^{-1} (u/v)$, where u is the zonal component and v is the meridional component. A wind blowing straight from the north is 0° , from the east is 90° , from the south is 180° , and from the west is 270° . The vertical velocity is either positive or negative, with positive being upwards and negative being downwards. This convention is adopted assuming the bulk flow is along isentropic surfaces. These surfaces generally slope upwards in the Northern Hemisphere, so a bulk flow up a surface is ascending, and is associated with instability, while flow

down a surface is descending, and is associated with stable conditions (Gage, 1983).

The baroclinicity δ is also positive or negative. Positive δ is associated with instability, while negative δ is associated with stability. It is a relative measure of the ratio of vertical to horizontal velocity, with a larger positive δ corresponding to greater instability and a larger negative δ corresponding to greater stability.

The plots of the horizontal speed and direction, and the zonal and meridional components can be easily compared to the LaSalle and Denver rawinsonde runs and the Platteville ST radar run. However, this is not the case with the vertical velocity, since none of these methods measures vertical velocity. This is because vertical velocity is difficult to measure. ST radars do not usually employ a vertical beam to measure this component, since the magnitudes are generally quite small, and can be assumed to be zero in many cases (Gage, 1983). Since there are no direct measurements of vertical velocities for comparison with MENTOR values, I used data derived by the U. S. Air Force Global Weather Central's High Resolution (HIRAS) Model for Denver at 18:00 UT. This data is derived from other fields measured by the 12:00 UT Denver rawinsonde, which is then input into a numerical model to generate the values for 18:00 UT. There are also no baroclinicity measurements to use as a comparison; as a matter of fact, I have not found a plot of baroclinicity

anywhere in the literature.

To generate these profiles, I used soundings comprised of 10 minutes of consecutive data. The zenith angle window was set at 24° to allow in as many points as possible. I used the linear polarization and least-squares polynomial filters mentioned in the last chapter, and used points within $\pm 2^\circ$ of zenith. The profiles generated don't contain as many points as the rawinsonde or ST radar runs, but do contain enough to paint a general picture of the atmospheric structure below 12 km. Also, the horizontal winds measured by the rawinsondes are normally accurate to within ± 1 m/s (Warnock et al., 1978), while there is no mention in the literature of the accuracy of the ST data. The accuracy of the rawinsonde method was challenged by Fukao and his co-workers (Fukao et al., 1982), who argued that differences between winds measured by MST radar and rawinsondes at Arecibo, Puerto Rico, were due mainly to inherent experimental errors in the rawinsonde technique. They went on to mathematically prove their theory.

Figures 19-22 show comparisons of the horizontal speed and direction, and zonal and meridional components from MENTOR data taken between 18:25:10 and 18:35:10 UT with the LaSalle rawinsondes and the Platteville ST radar. Note the terms LORAN and OMEGA; these refer to two different techniques used to determine wind velocities using rawinsondes. There is good agreement between the profiles of horizontal speed and direction. One must remember that

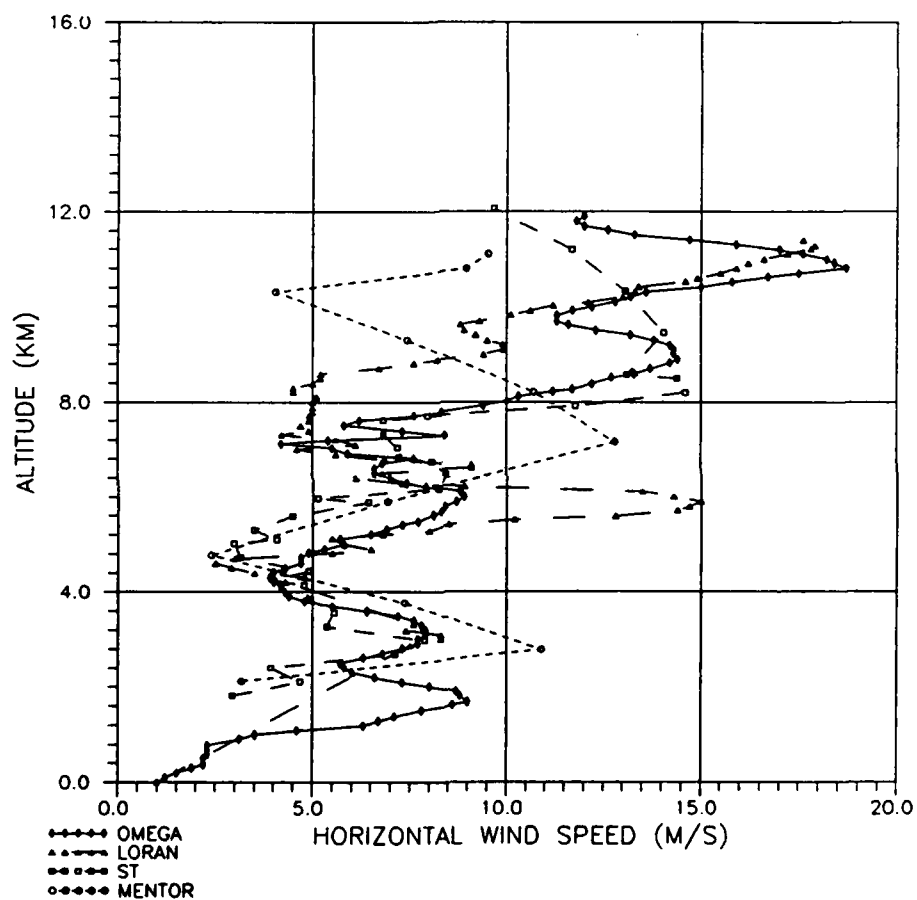


Fig. 19. A comparison of horizontal wind speeds determined by the 18:25:10-18:35:10 MENTOR data, the LaSalle rawinsondes, and the Platteville ST radar.

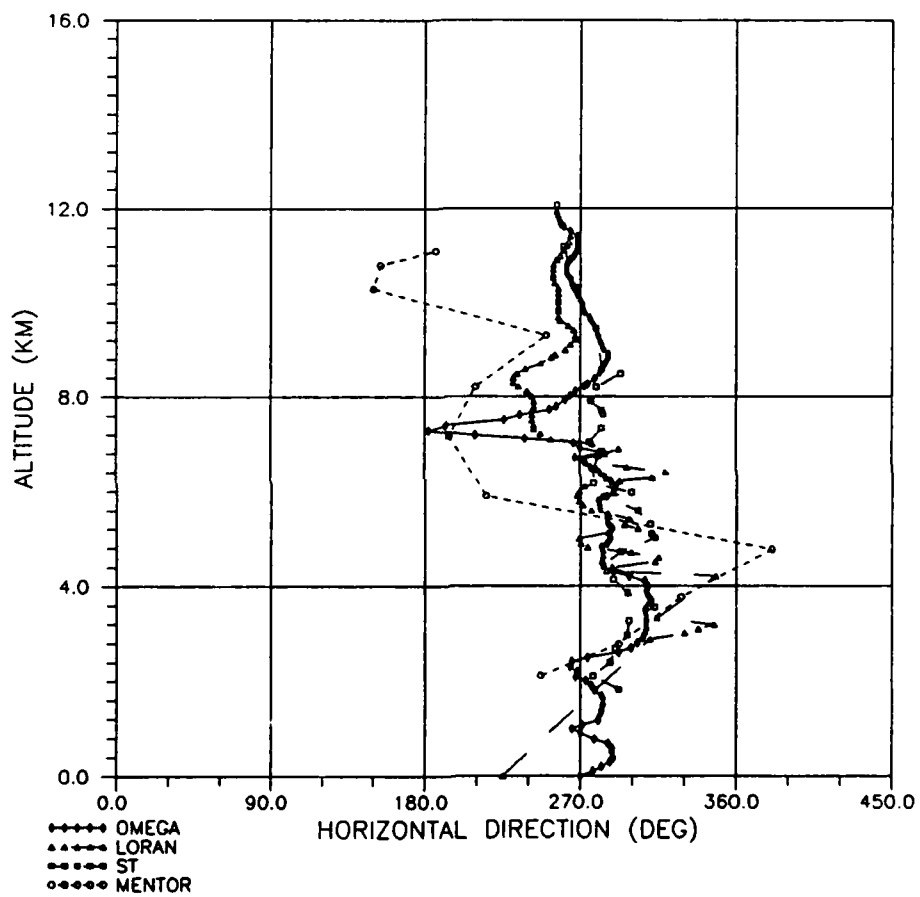


Fig. 20. A comparison of horizontal directions determined by the 18:25:10-18:35:10 MENTOR data, the LaSalle rawinsondes, and the Platteville ST radar.

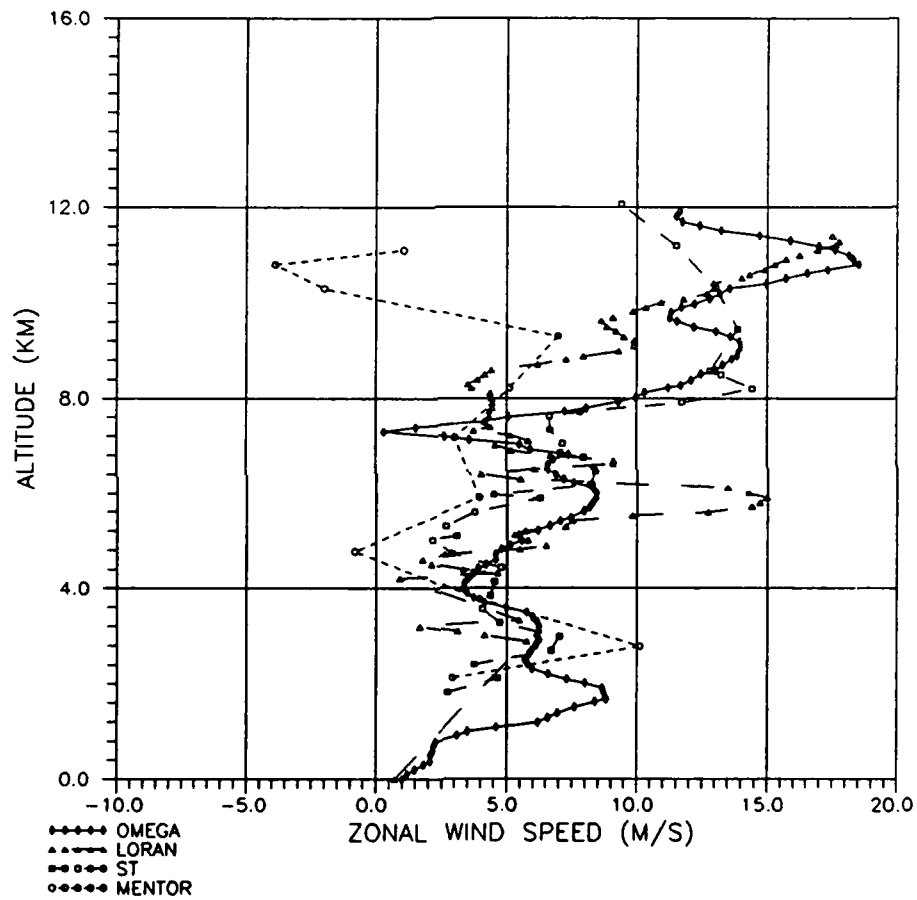


Fig. 21. A comparison of zonal wind speeds determined by the 18:25:10-18:35:10 MENTOR data, the LaSalle rawinsondes, and the Platteville ST radar.

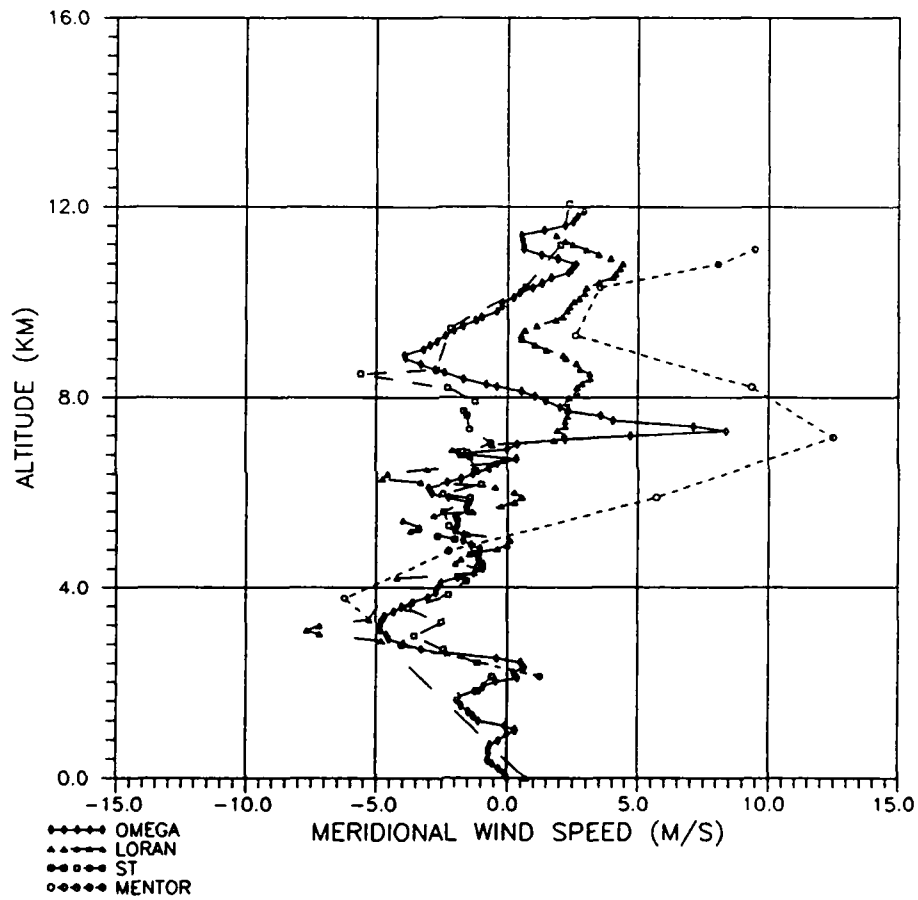


Fig. 22. A comparison of meridional wind speeds determined by the 18:25:10-18:35:10 MENTOR data, the LaSalle rawinsondes, and the Platteville ST radar.

the resolution on the MENTOR data is not as good as it could be if the system was able to measure points further off-zenith. The MENTOR profile follows the general trend given by the other techniques. There is a large discrepancy in direction above 10 km, but one must always keep in mind that each of these soundings was taken at a different time using different techniques and types of equipment. Not only are there experimental errors which are inherent in any measurement, but the atmosphere is extremely dynamic. Turbulent eddies are created and destroyed in time scales on the order of seconds. These eddies transfer horizontal momentum vertically, which produces fluctuations in the horizontal wind flow. Therefore one can expect to see differences in the profiles; the rawinsonde and ST data do not even agree totally. The discrepancy in the direction is due to the difference in the zonal component measured by MENTOR. It measured a small easterly component (speeds less than zero are easterly) where the others measured relatively large westerlies. It's interesting to note the good agreement in measurements of the meridional component in Figure 22. The strong directional shear noted in Figure 20 and the corresponding shear in the meridional component could be an indication of an upward-propagating mountain lee wave. Figures 23-26 show the same MENTOR data compared against the Denver rawinsonde data. Once again, there is fairly good agreement between the profiles, even though 6 hours separate

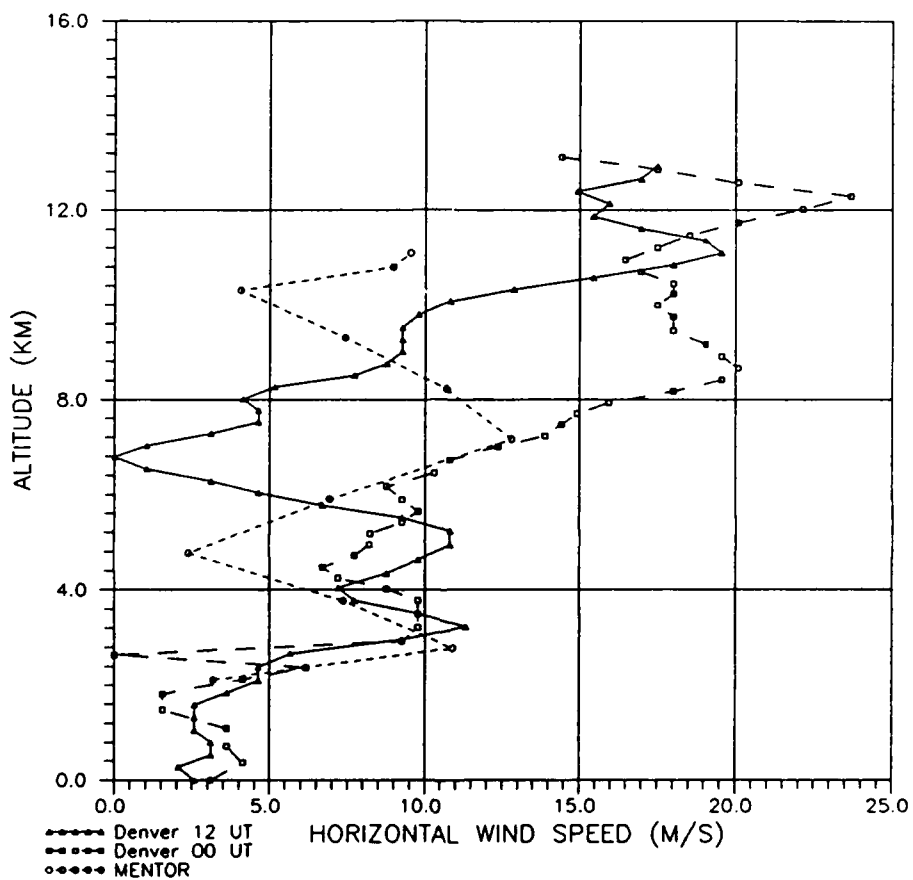


Fig. 23. A comparison of horizontal wind speeds determined by the 18:25:10-18:35:10 MENTOR data and the Denver rawinsondes.

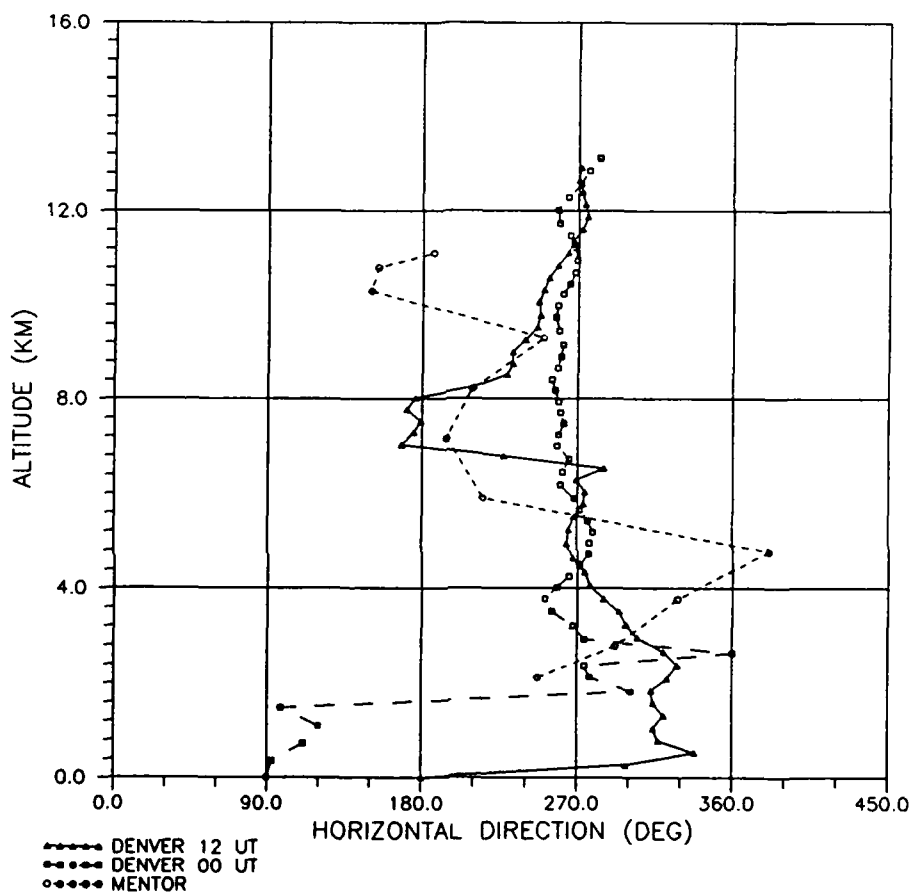


Fig. 24. A comparison of horizontal directions determined by the 18:25:10-18:35:10 MENTOR data and the Denver rawinsondes.

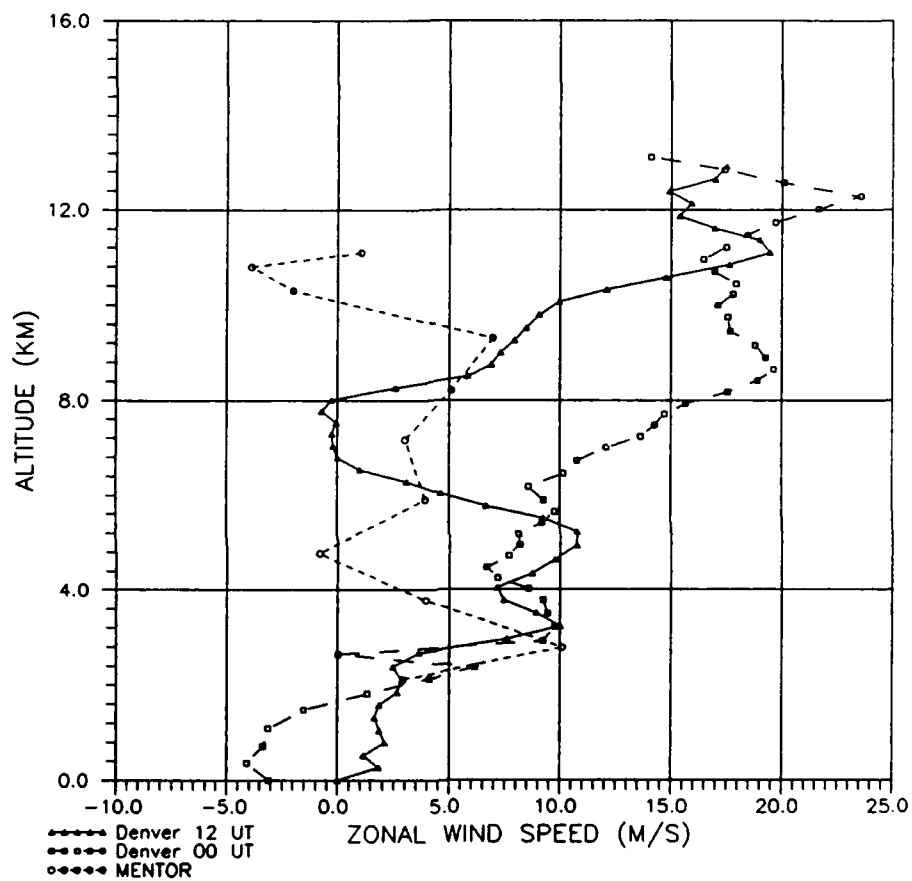


Fig. 25. A comparison of zonal wind speeds determined by the 18:25:10-18:35:10 MENTOR data and the Denver rawinsondes.

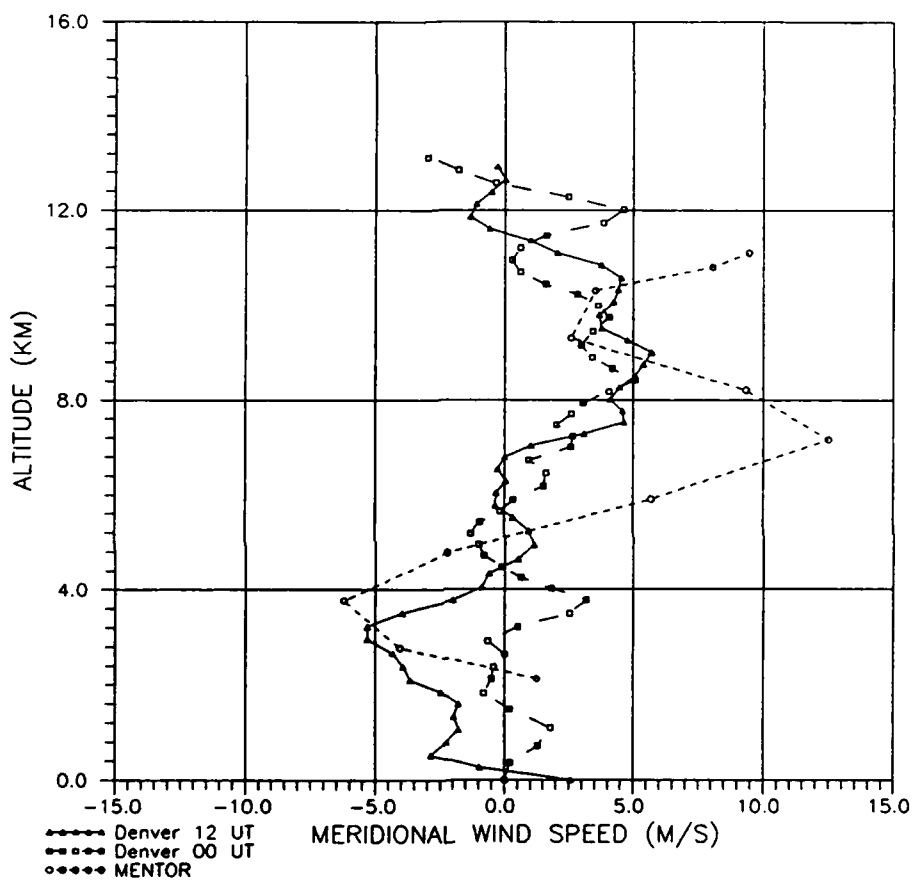


Fig. 26. A comparison of meridional wind speeds determined by the 18:25:10-18:35:10 MENTOR data and the Denver rawinsondes.

the MENTOR profile from each Denver one. Also, the two sites are about 60 miles apart. Denver is at the base of the Rockies while LaSalle is on the high plains. There are more discrepancies in all the profiles, but that should be expected in this case. Figure 27 is a comparison of vertical velocity from MENTOR with those derived from the HIRAS model. These are very good results, since they both show upward vertical motion and the magnitudes are similar. This result would indicate that the MENTOR is well suited to measure vertical velocities. Figure 28 shows a plot of baroclinicity from MENTOR. The high positive value near 2 km would indicate strong instability, with increasing stability above that until just below 10 km.

Figures 29-32 are comparisons of the wind profiles generated by MENTOR data from 18:45:10 to 18:55:10 UT, the LaSalle rawinsondes and the Platteville ST radar. Since there were not as many points in this 10 minute sounding as there were in the previous one, there are not as many points in its profile. This may also explain why the results are not as good as those obtained 10 minutes earlier. For example, Figure 29 shows a large increase in winds between 3.6 km and 5.2 km. It's possible that this would not appear if there were more data to work with; more data would improve the resolution. However, the data does follow the general trend well, especially the increase at 5.2 km, which was also detected by the LORAN rawinsonde out of LaSalle. The

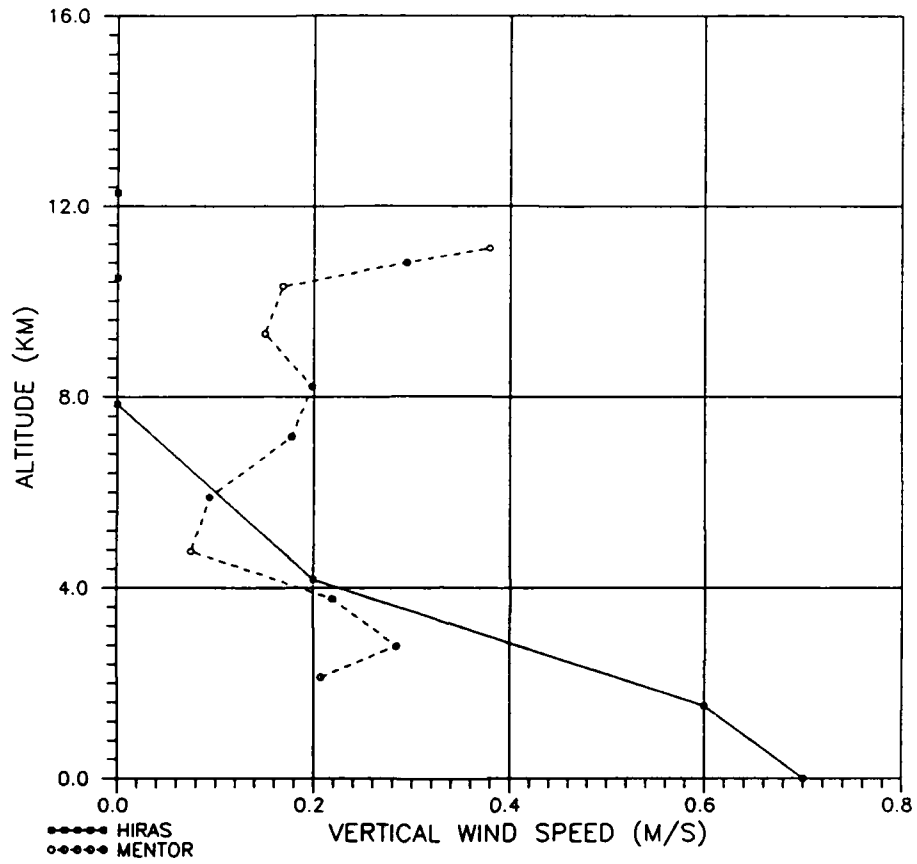


Fig. 27. A comparison of vertical velocities determined by the MENTOR 18:25:10-18:35:10 data and the AFGWC HIRAS model for Denver.

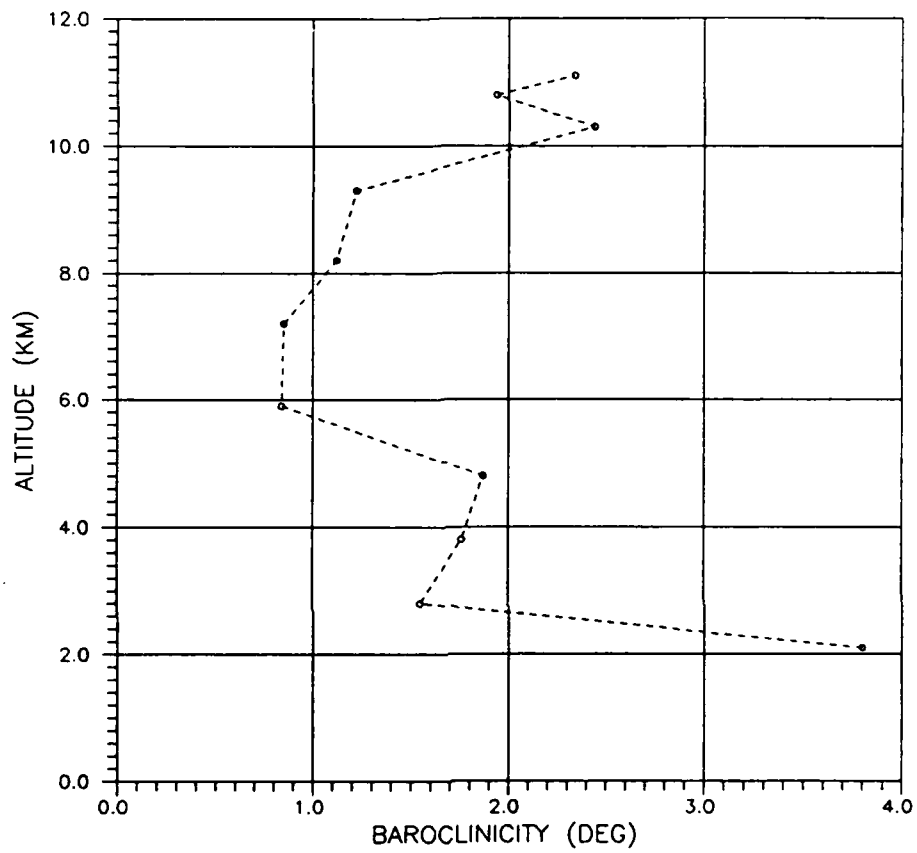


Fig. 28. Plot of baroclinicity vs. altitude from the MENTOR 18:25:10-18:35:10 data.

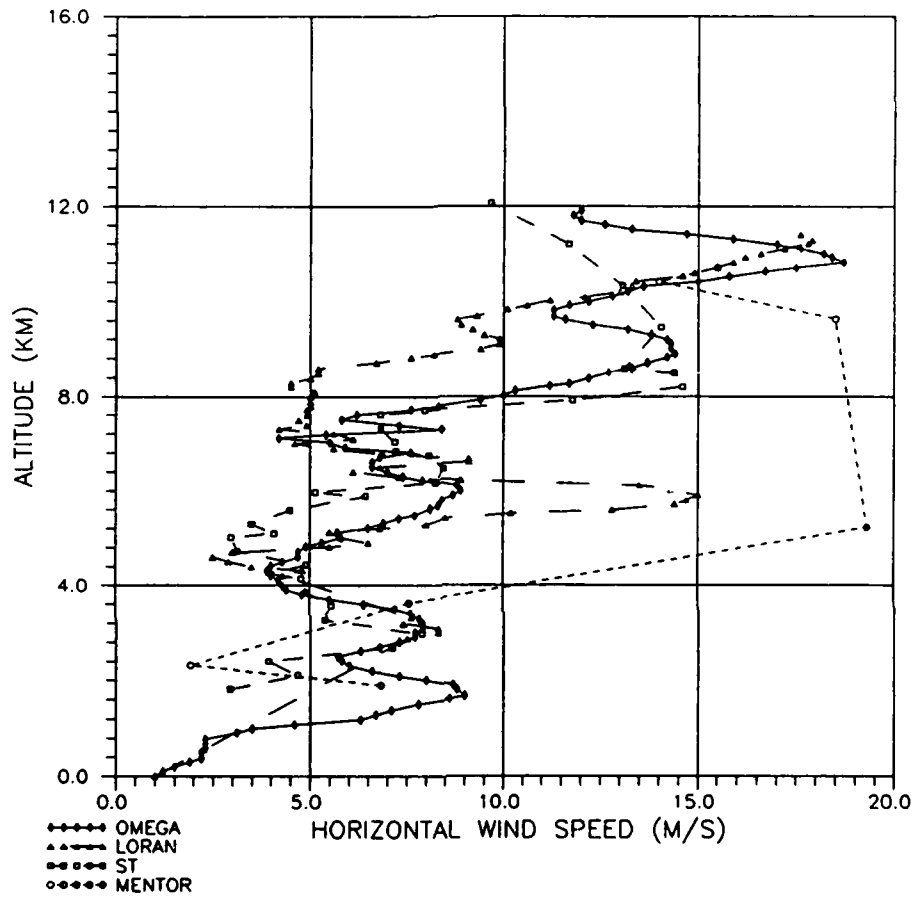


Fig. 29. A comparison of horizontal wind speeds determined by the MENTOR 18:45:10-18:55:10 data, the LaSalle rawinsondes, and the Platteville ST radar.

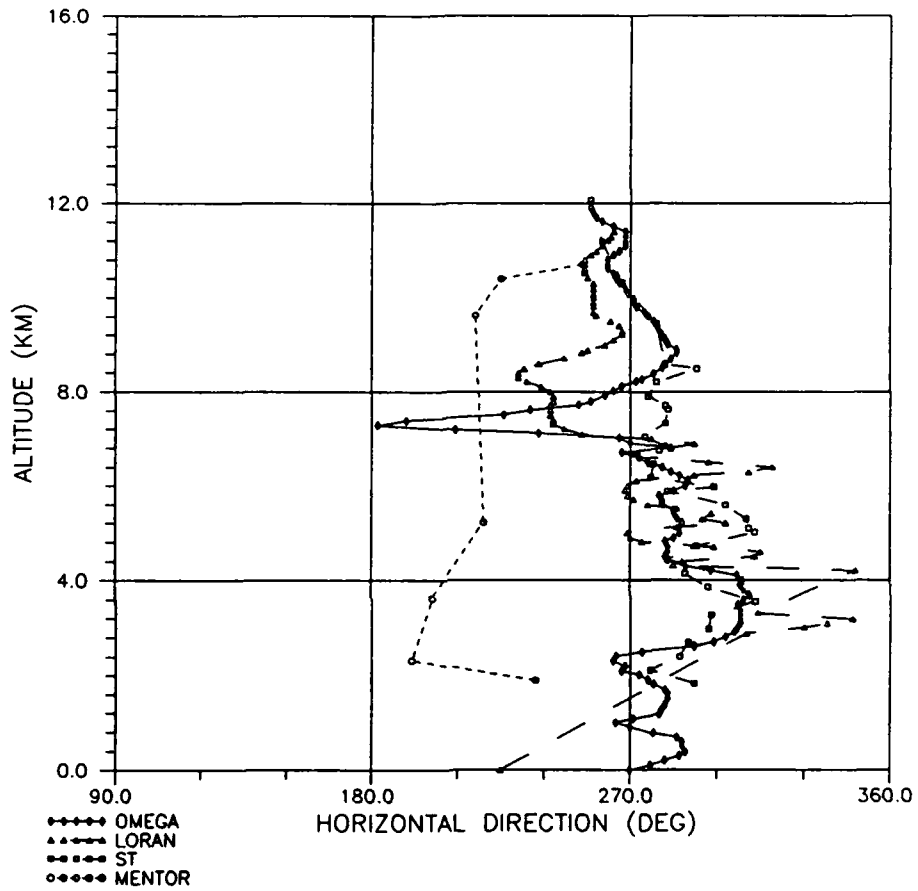


Fig. 30. A comparison of horizontal directions determined by the MENTOR 18:45:10-18:55:10 data, the LaSalle rawinsondes, and the Platteville ST radar.

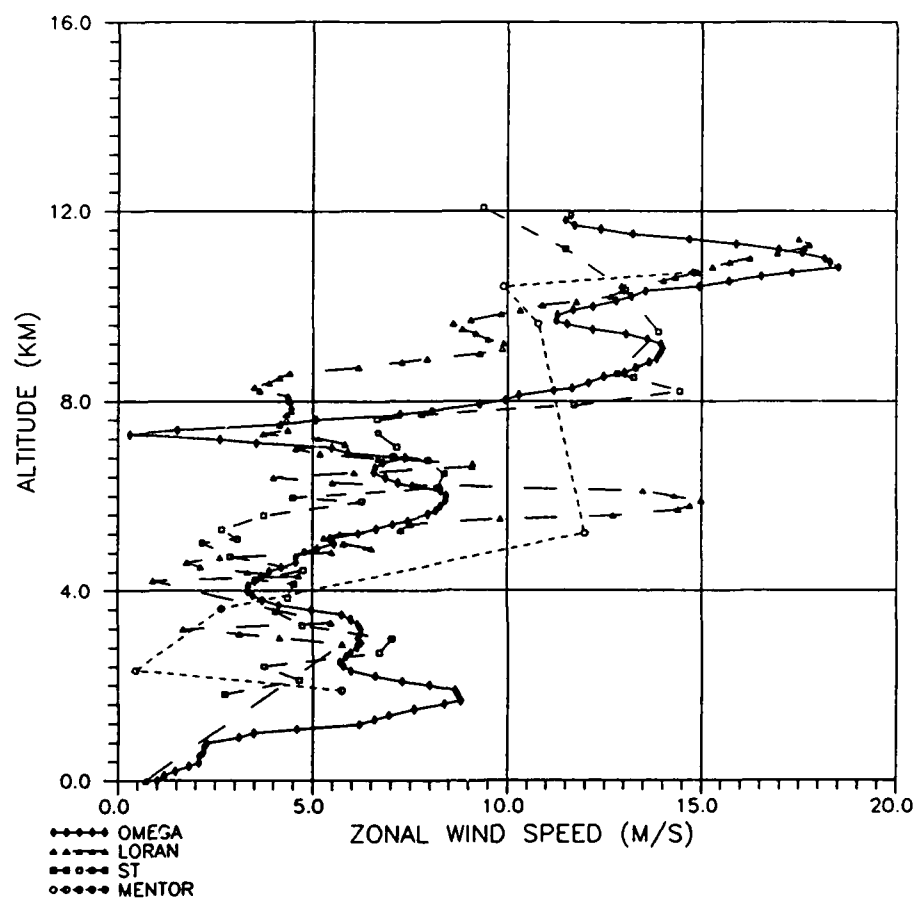


Fig. 31. A comparison of zonal wind speeds determined by the MENTOR 18:45:10-18:55:10 data, the LaSalle rawinsondes, and the Platteville ST radar.

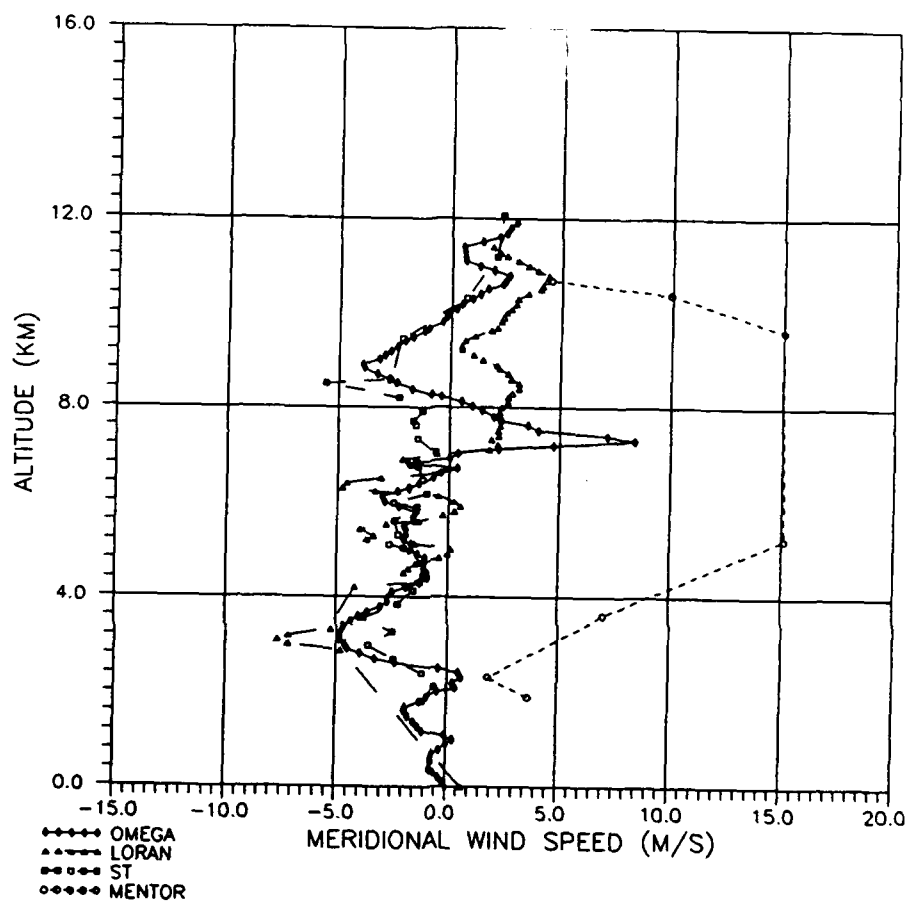


Fig. 32. A comparison of meridional wind speeds determined by the MENTOR 18:45:10-18:55:10 data, the LaSalle rawinsondes, and the Platteville ST radar.

horizontal directions obtained this time around to not agree as well as those 10 minutes earlier. This is mainly caused by the discrepancy in meridional components measured by MENTOR and by the other techniques (see Figure 32). The only good agreement is at the lowest and highest altitudes. Otherwise, MENTOR measures high southerly components, while the others measure relatively small northerly components. MENTOR and the LORAN rawinsonde do correlate somewhat on the strong southerly component at 5.2 km. Figure 30 shows that the directions measured by MENTOR are for the most part within 90° of those measured by the other methods. Figure 31 shows that there is good agreement on the zonal components measured by each method. The same arguments used in describing the first set of MENTOR data comparisons can be used here as well. It demonstrates how turbulent and chaotic the atmosphere is. Figures 33-36 show this MENTOR profile compared to those from the Denver rawinsondes. Figure 33 shows some discrepancy in the horizontal wind measured at 5.2 km, but otherwise good agreement. Once again, better resolution could solve this problem. The horizontal directions in Figure 34 once again show the MENTOR profile offset from the others by about 30° - 60° ; note the strong directional shear measured by the 12:00 UT rawinsonde. This is an indication of how quickly the atmosphere can change, and is possibly another indication of an upward-propagating mountain lee wave. It is possible that the MENTOR does pick

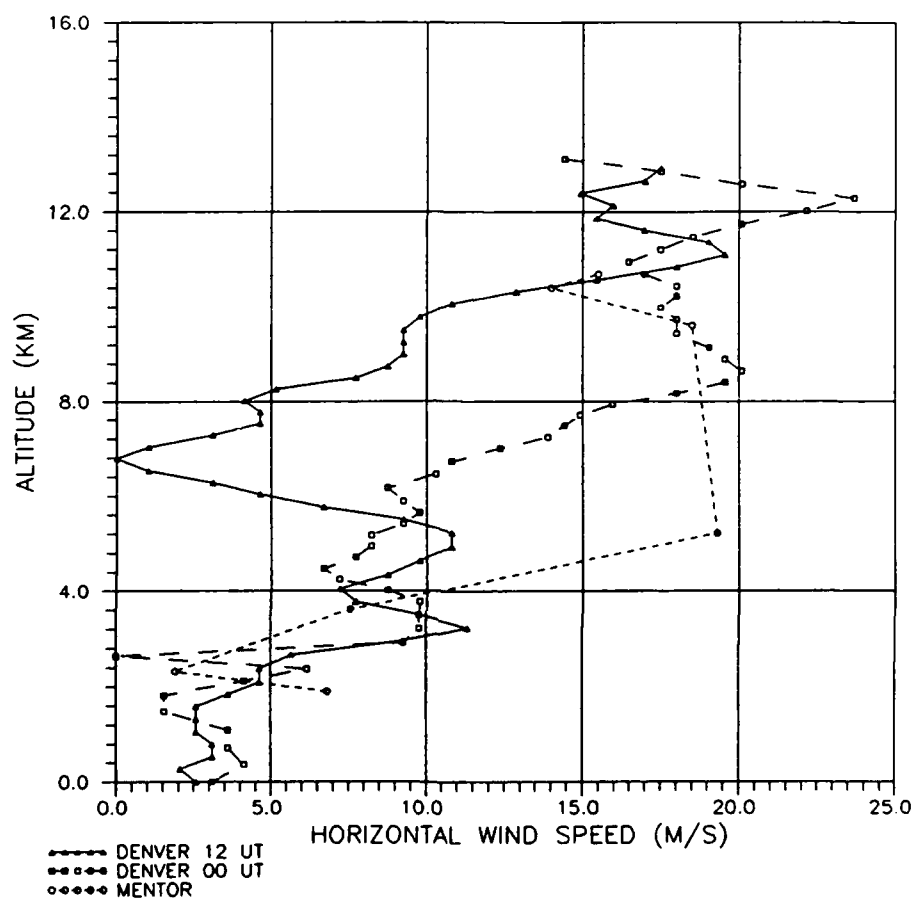


Fig. 33. A comparison of horizontal wind speeds determined by the MENTOR 18:45:10-18:55:10 data and the Denver rawinsondes.

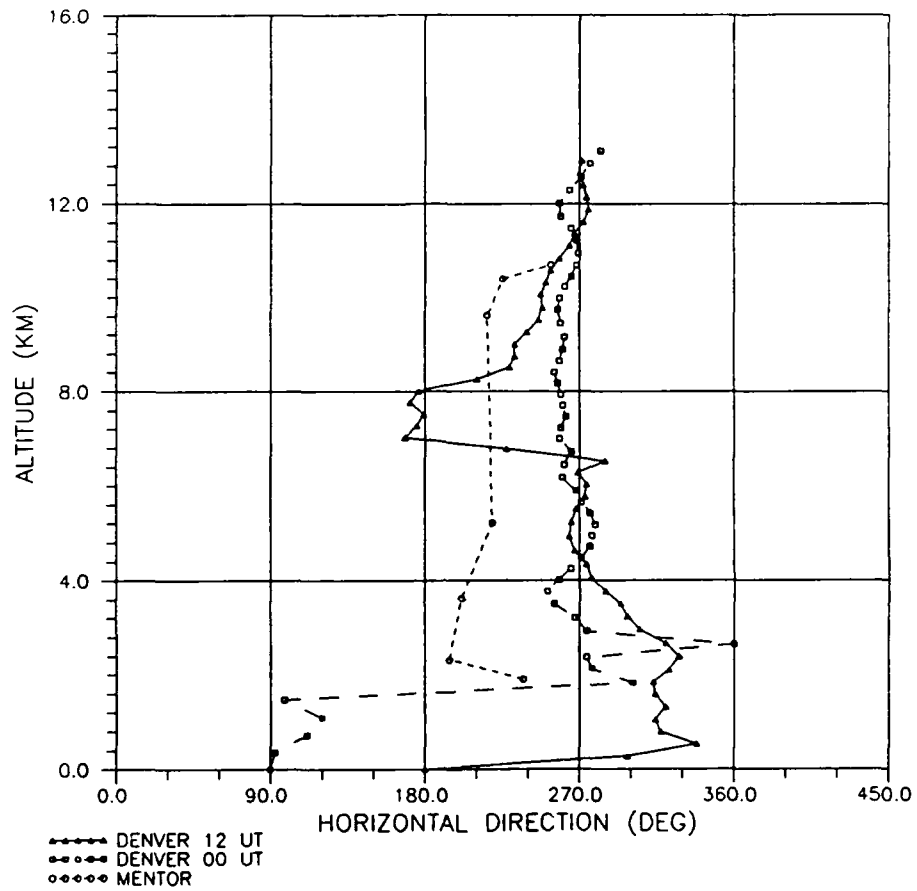


Fig. 34. A comparison of horizontal directions determined by the MENTOR 18:45:10-18:55:10 data and the Denver rawinsondes.

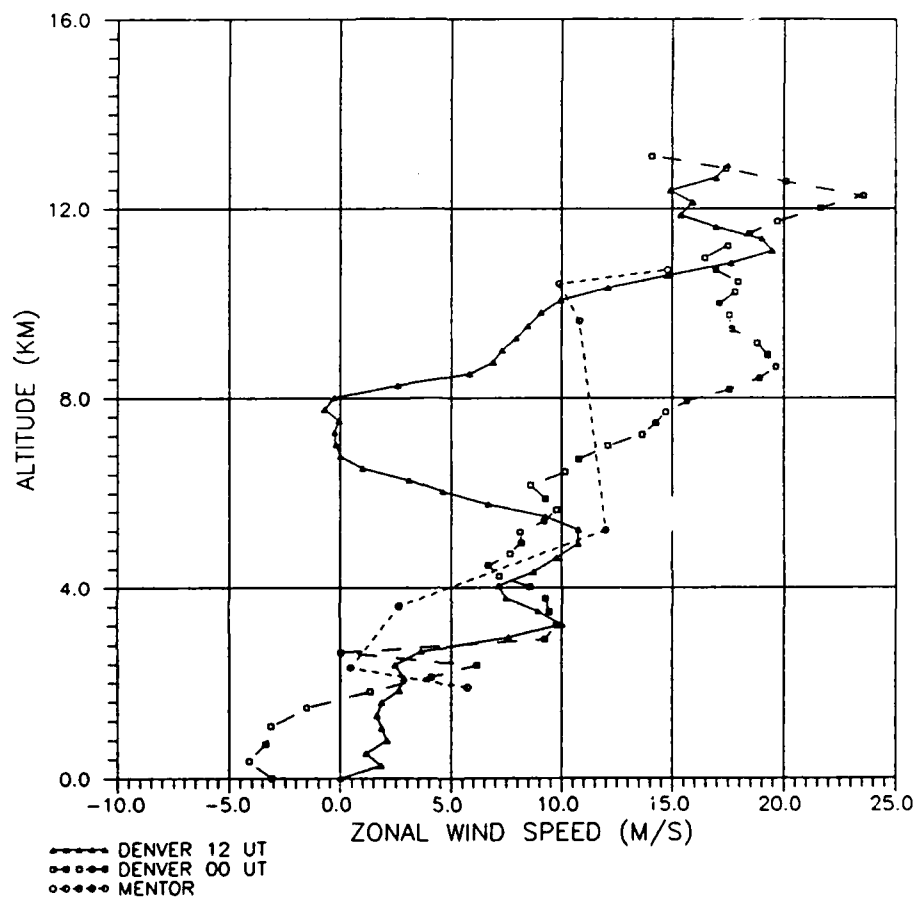


Fig. 35. A comparison of zonal wind speeds determined by the MENTOR 18:45:10-18:55:10 data and the Denver rawinsondes.

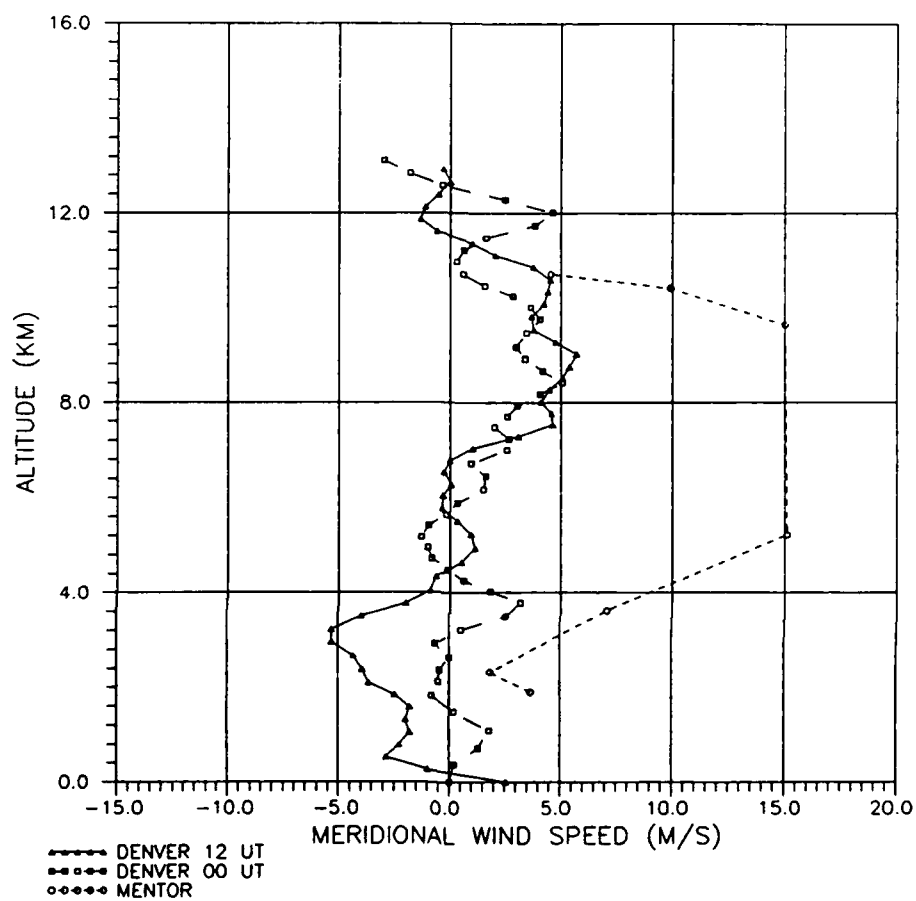


Fig. 36. A comparison of meridional wind speeds determined by the MENTOR 18:45:10-18:55:10 data and the Denver rawinsondes.

up this wave motion, but due to the long sounding times and the effects of smearing, does not show the sharp distinction, but rather a smoother directional variation with height. One can see from Figures 35 and 36 that there is pretty good agreement between the zonal components but not as much between the meridional components. Figure 37 shows the comparison between vertical velocities from MENTOR and the HIRAS model. There is once again good agreement here, and it appears that the MENTOR has detected a wave with a vertical wavelength of about 8 km. One could make a case for this being a gravity wave that was generated by the Rockies, since not only is there vertical evidence of propagation but possibly some evidence of horizontal propagation as well. Figure 38 is a plot of baroclinicity, and shows that the atmosphere is stable between 3.8 km and 10 km, and highly unstable near 2 km. This instability could enhance the gravity wave at low altitudes, and the resultant stability from 3.8 to 10 km is not enough to damp it.

One can also compare the two soundings generated by the MENTOR to see if the differences can be attributed to meteorological phenomena. In comparing the horizontal speed along with its zonal and meridional components, one can see evidence of a horizontally-propagating mountain lee wave. It appears that the zonal component was perturbed in the first profile between 3-5 km and 9-11 km. These altitudes are where the zonal component becomes easterly. The

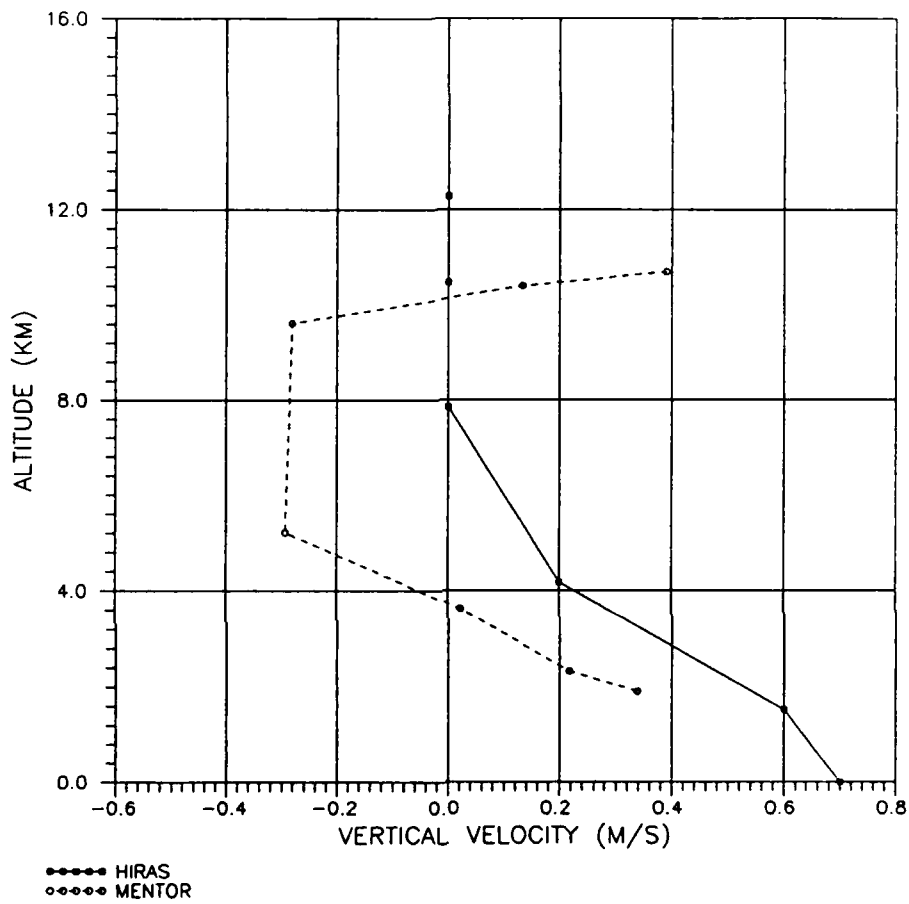


Fig. 37. A comparison of vertical velocities determined by the MENTOR 18:45:10-18:55:10 data and the AFGWC HIRAS model for Denver.

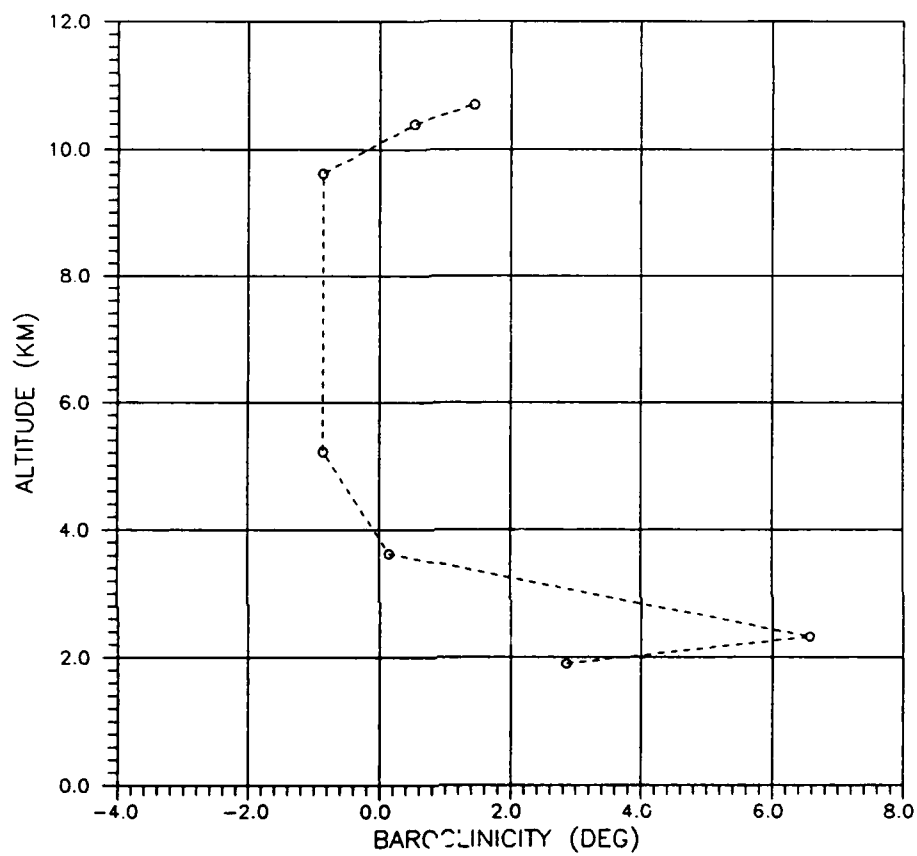


Fig. 38. Plot of baroclinicity vs. altitude from the MENTOR 18:45:10-18:55:10 data.

meridional component also shows evidence of this wave at the same altitudes in the first profile. This is evident by the shift to a more northerly component at these altitudes. The strong directional shear also points to a wave. It appears that the wave was propagating vertically also; as the second profile of vertical velocity shows. Coincidentally, the amplitude peaks are at 3 km and 11 km.

A quick error analysis of the two profiles showed that the average standard deviations of V_H , u , and v were 4.35 m/s, 4.64 m/s, and 4.14 m/s, respectively, while that of α was 9.83'. These are well within acceptable meteorological standards, especially considering the wave activity. The average standard deviation of w was 0.14 m/s, which is exceptional. This further verifies that MENTOR provides extremely accurate vertical velocity measurements. The average standard deviation of δ was 0.85'. While there is no standard by which to compare, the fact that the vertical and horizontal components compared well indicate MENTOR also provides accurate baroclinicity measurements.

Unfortunately, the lack of continuous data and the amount of continuous data needed to generate wind profiles makes it impossible to show plots of winds with time. These would provide the chance to see changing winds due to various meteorological phenomena as well as atmospheric wave motions.

CHAPTER V

CONCLUSIONS AND RECOMMENDATIONS

One can conclude from the results that the MENTOR does indeed provide reasonable wind profiles of the lower atmosphere. The results are not as accurate as one would like, but this radar is new, and like anything new, it must be tested and developed to further refine it and to make it useful. It was not originally designed to measure lower atmospheric winds, but to use meteor echoes to measure upper atmospheric winds. All the profiles seem to indicate that the MENTOR is not subject to the finite range volume effect described in Chapter 3. If it were, there would have been large horizontal wind shears measured over a very small altitude range, on the order of 40 meters per second per kilometer (Fukao et al., 1988). However, this effect was first discovered on an MST radar. The Platteville ST radar did not appear to be affected by it either. More than likely, the conditions were not right for this effect to occur.

The problem of the distinct power drop-off at more than 2° off-zenith also hinders the calculation of horizontal velocities. A small decrease in frequency would provide a wider beam and could provide better horizontal velocity measurements.

This decrease in frequency could allow the collection of more useful points, which would cut down the number of consecutive soundings needed to provide a profile as well as increase the vertical resolution. The frequency decrease may sacrifice some of the lower altitude information, but the increased resolution could account for most of that.

Another area of potential is the development of a desmearing routine, which would take into account the movement of scatterers across different Fourier windows as they move through the radar beam. This would improve the accuracy of the winds that are calculated.

There is also the problem of the missing y-component on one of the antennas. Although filtering of the data probably removed most of the bad points, fixing this problem could also improve the accuracy.

I believe that the calculation of baroclinicity could be useful to determine the atmospheric stability at various times, and could be a useful input parameter to baroclinic numerical weather prediction models.

With the MENTOR in its present configuration, I found that it's best to use a 10-minute sounding, a linear polarization filter in conjunction with doing an FFT on the time domain data, filtering points using a least-squares polynomial fit to a plot of radial zenith angle versus radial velocity calculated by coherently averaging over one minute, and finally filtering out all points outside $\pm 2^\circ$ off-zenith.

A zenith angle window of 24° worked best, and anything less than that just doesn't allow in enough points to plot an adequate profile. The inclusion of extremely fast data processing hardware and software will make it possible for MENTOR to generate these profiles quickly, thus making them much more current and therefore more useful to those that require real-time wind information. The current rawinsonde network only provides this information every 12 hours; the data is old 30 minutes after it's gathered.

As a final note, if all these suggestions do indeed produce good results, then the MENTOR can then be included with the ST and SAD methods for measuring atmospheric winds. There are also possibilities for detecting wave motions as well. Best of all, the MENTOR is much smaller, requires less power, and is more transportable than either of the others. It could become a cost-effective alternative to the expensive rawinsonde network and the other radars.

REFERENCES

- Adams, G. W., D. P. Edwards, and J. W. Brosnahan, The imaging Doppler interferometer: Data analysis, Radio Sci., 20, 1481-1492, 1985
- Adams, G. W., J. W. Brosnahan, D. C. Walden, and S. F. Nerney, Mesospheric observations using a 2.66-MHz radar as an Imaging Doppler Interferometer: Description and First Results, J. Geophys. Res., 91, 1671-1683, 1986.
- Balsley, B. B., Design Considerations for coherent radar systems for probing the troposphere, stratosphere, and mesosphere, Preprint Volume on the 18th Conference on Radar Meteorology, March 28-31, 1978, Atlanta, Georgia, 387-390, 1978.
- Balsley, B. B., The MST technique-A brief review, J. Atmos. Terr. Phys., 43, 495-509, 1981.
- Balsley B. B., and K. S. Gage, On the vertical-incidence VHF backscattered power profile from the stratosphere, Geophys. Res. Lett., 8, 1173-1175, 1981.
- Battan, L. J., Radar Observations of the Atmosphere, pp. 10-20, 267, University of Chicago Press, Chicago, 1973.
- Briggs, B. H., Radar observations of atmospheric winds and turbulence: a comparison of techniques, J. Atmos. Terr. Phys., 42, 823-833, 1980.
- Brosnahan, J. W., G. W. Adams, J. W. Neuschaefer, and D. M. Woodard, The MAPSTAR 2.66-MHz Imaging Doppler Interferometer Radar, CASS Report GR-09, Utah State University, Logan, 1987.
- Brosnahan, J. W., G. W. Adams, J. W. Neuschaefer, D. M. Woodard, and R. G. Roper, The MAPSTAR and MENTOR Imaging Doppler Interferometer Radars, COSPAR 1988, Paper No. VI.1.6, 1-9, 1988.
- Byers, H. R., General Meteorology, pp. 427-432, McGraw Hill, New York, 1974.
- Doviak, R. J., and D. S. Zrnic, Doppler Radar and Weather Observations, pp. 24-28, 359-433, Academic Press, Orlando, 1984.
- Fukao, S., T. Sato, P. T. May, T. Tsuda, S. Kato, M. Inaba, and I. Kimura, A systematic error in MST/ST radar wind measurement induced by a finite range volume effect. I. Observational results, Radio Sci., 23, 59-73, 1988.

Fukao, S., T. Sato, N. Yamasaki, R. M. Harper, and S. Kato, Winds measured by a UHF Doppler radar and rawinsondes: Comparisons made on twenty-six days (August-September 1977) at Arecibo, Puerto Rico, J. Appl. Meteorol., 21, 1357-1363, 1982.

Gage, K. S., and B. B. Balsley, On the scattering and reflection mechanisms contributing to clear air radar echoes from the troposphere, stratosphere, and mesosphere, Radio Sci., 15, 243-257, 1980.

Gage, K. S., On the measurement of vertical velocity by MST radar, Handbook for MAP, Vol. 9, edited by S. A. Bowhill and B. Edwards, pp. 215-226, SCOSTEP Secretariat, University of Illinois, Urbana, 1983.

Gage, K. S., B. B. Balsley, and J. L. Green, Fresnel scattering model for the specular echoes observed by VHF radar, Radio Sci., 16, 1447-1453, 1981.

Gage, K. S., and T. E. VanZandt, Wind measurement techniques available for the middle atmosphere program, J. Geophys. Res., 86 (C 10), 9591-9598, 1981.

Gage, K. S., and G. D. Nastrom, On the spectrum of atmospheric velocity fluctuations seen by MST/ST radar and their interpretation, Handbook for MAP, Vol. 14, edited by S. A. Bowhill and B. Edwards, pp. 197-207, SCOSTEP Secretariat, University of Illinois, Urbana, 1984.

Holton, J. R., An Introduction to Dynamic Meteorology, pp. 51-52, 99-100, Academic Press, New York, 1972.

Ierkic, H. M., and J. Röttger, Mesospheric measurements of irregularity patches using a 3-antenna interferometer, Handbook for MAP, Vol. 14, edited by S. A. Bowhill and B. Edwards, pp. 174-178, SCOSTEP Secretariat, University of Illinois, Urbana, 1984.

Panofsky, H. A., and J. A. Dutton, Atmospheric Turbulence, pp. 176-179, John Wiley and Sons, New York, 1984.

Röttger, J., and C. H. Liu, Partial reflection and scattering of VHF radar signals from the clear atmosphere, Geophys. Res. Lett., 5, 357-360, 1978.

Röttger, J., P. Czechnowsky, and G. Schmidt, First low-power VHF radar observations of tropospheric, stratospheric, and mesospheric winds and turbulence at the Arecibo Observatory, J. Atmos. Terr. Phys., 43, 789-800, 1981.

Röttger, J., The MST Radar Technique, Handbook for MAP, Vol. 13, edited by S. A. Bowhill and B. Edwards, pp. 187-232, SCOSTEP Secretariat, University of Illinois, Urbana, 1984.

Röttger, J., and H. M. Ierkic, Postset beam steering and interferometer applications of VHF radars to study winds, waves, and turbulence in the lower and middle atmosphere, Radio Sci., 20, 1461-1480, 1985.

Royrvik, O., Implication on data interpretation by short- and long-period oscillations, Handbook for MAP, Vol. 9, edited by S. A. Bowhill and B. Edwards, pp. 228-231, SCOSTEP Secretariat, University of Illinois, Urbana, 1983.

Smith, S. A., and D. C. Fritts, Poker Flat MST radar and meteorological rocketsonde wind profile comparisons, Geophys. Res. Lett., 11, 538-540, 1984.

Tsuda, T., T. Sato, K. Hirose, S. Fukao, and S. Kato, MU radar observations of the aspect sensitivity of backscattered VHF echo power in the troposphere and lower stratosphere, Radio Sci., 21, 971-980, 1986.

Vincent, R. A., Relationship of Spaced Antenna and Doppler techniques for velocity measurements, Handbook for MAP, Vol. 14, edited by S. A. Bowhill and B. Edwards, pp. 125-129, SCOSTEP Secretariat, University of Illinois, Urbana, 1984.

Vinnichenko, N. K., N. Z. Pinus, S. M. Shmeter, and G. N. Shur, Turbulence in the Free Atmosphere, pp. 97-119, Consultants Bureau, New York, 1980.

Warnock, J. M., T. E. VanZandt, J. L. Green, and R. H. Winkler, Comparison between wind profiles measured by Doppler radar and by rawinsonde balloons, Geophys. Res. Lett., 5, 109-112, 1978.

Waterman, A. T., T-z. Hu, P. Czechowsky, and J. Röttger, Variability in Doppler slant-beam measurement of horizontal wind: A case study, Radio Sci., 20, 1214-1222, 1985.

Woodman, R. F., and A. Guillen, Radar observations of winds and turbulence in the stratosphere and mesosphere, J. Atmos. Sci., 31, 493-505, 1974.

APPENDIX

88 AUG 22 P 102
 10 August 1988
 Michael J. Volek
 771 N. 500 E. Bsmt. R.
 Logan UT 84321
 (801) 753-2148

Dear Sir:

I am in the process of preparing my thesis in the Soil Science and Biometeorology Department at Utah State University. I hope to complete in the Spring of 1989.

I am requesting your permission to include the attached material as shown. I will include acknowledgments and/or appropriate citations to this work as shown and copyright and reprint rights information in a special appendix. The bibliographical citation will appear at the end of the manuscript as shown. Please advise me of any changes required.

Please indicate your approval of this request by signing in the space provided, attaching any other form or instruction necessary to confirm permission. If you charge a reprint fee for use of your material, please indicate that as well. If you have any questions, please call me at the number above.

The first attachment is a figure from a paper by K. S. Gage and T. E. VanZandt (paper #1C0557, Vol 86 (C10), pp 9591-9598). The others are from a paper by Adams et al (paper #5A8550, Vol 91 (A2), pp 1671-1683). Dr Adams is my thesis advisor, and has already given his permission; however, I need your approval as copyright holder to reproduce this material for my use.

I hope you will be able to reply immediately. Thank you for your cooperation.

Michael J. Volek

I hereby give permission to Michael J. Volek to reprint the following material in his thesis:

Gage, K. S., and T. E. VanZandt, 1981: Wind measurement techniques available for the middle atmosphere program. Journal of Geophysical Research, 86 (C 10), 9591-9598.

Adams, G. W., J. W. Brosnahan, D. C. Walden, and S. F. Nerney, 1986: Mesospheric observations using a 2.66-MHz radar as an Imaging Doppler Interferometer: Description and First Results. Journal of Geophysical Research. 91 (A2), 1671-1683.

Patty Robinson
 ABLL
 8/23/88

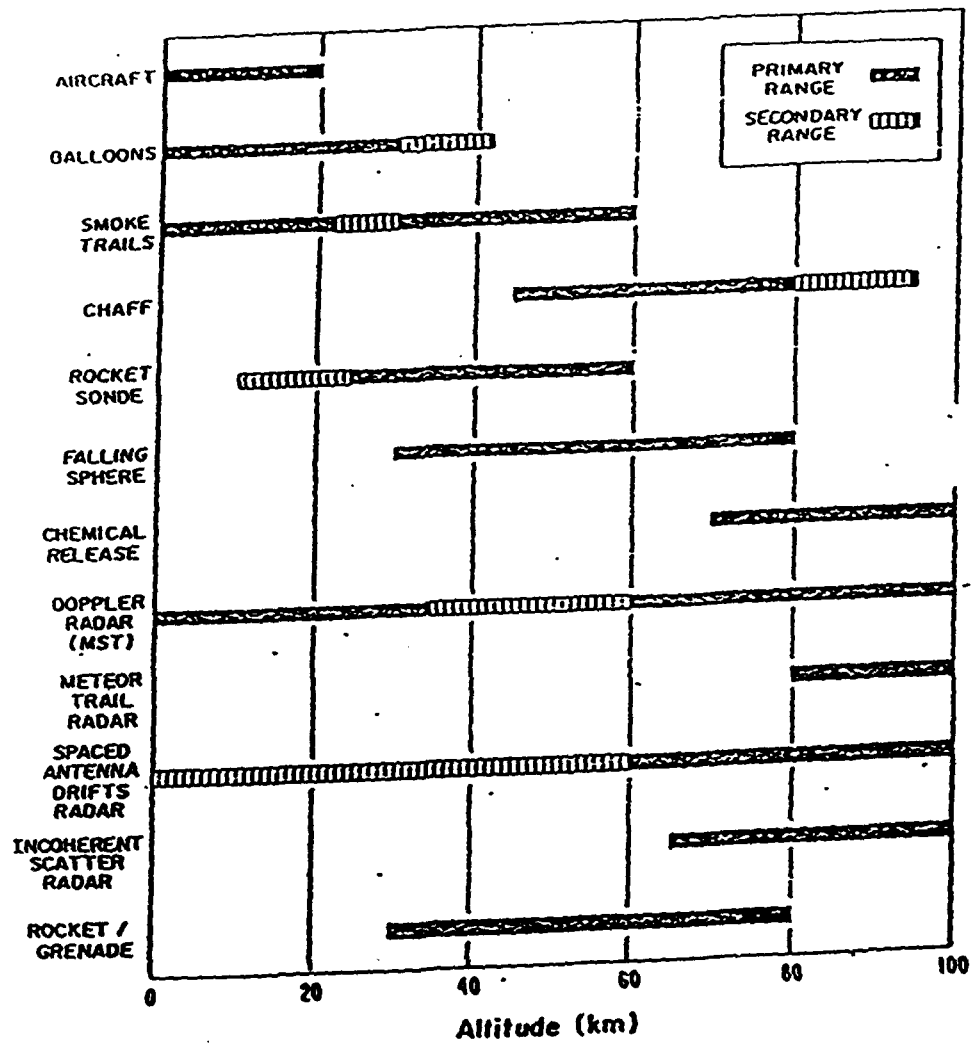


Fig. 1. Various atmospheric wind measurement techniques. (From Gage and Van Zandt, 1981.)

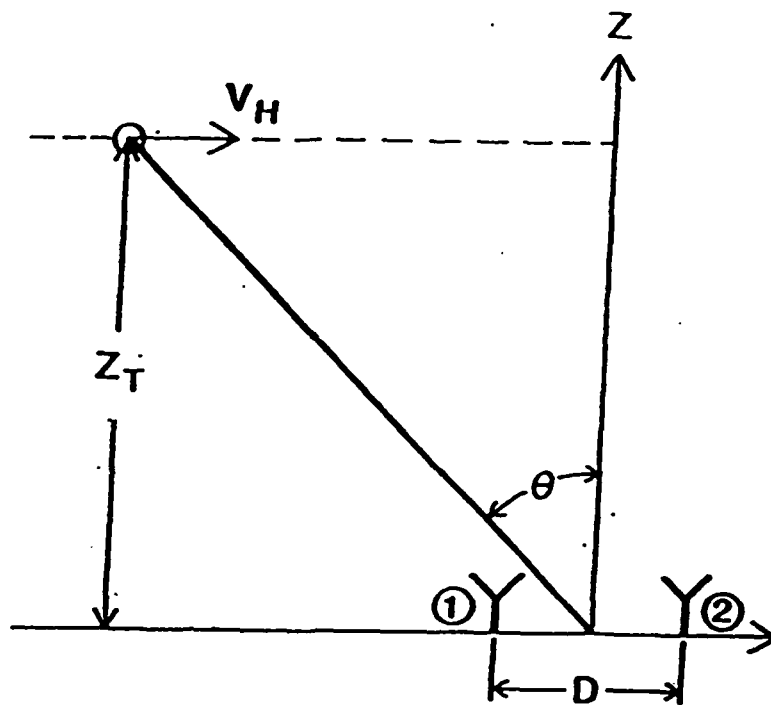


Fig. 3. Geometry for single horizontally moving target being viewed by a two-antenna interferometer. (From Adams et al., 1985.)

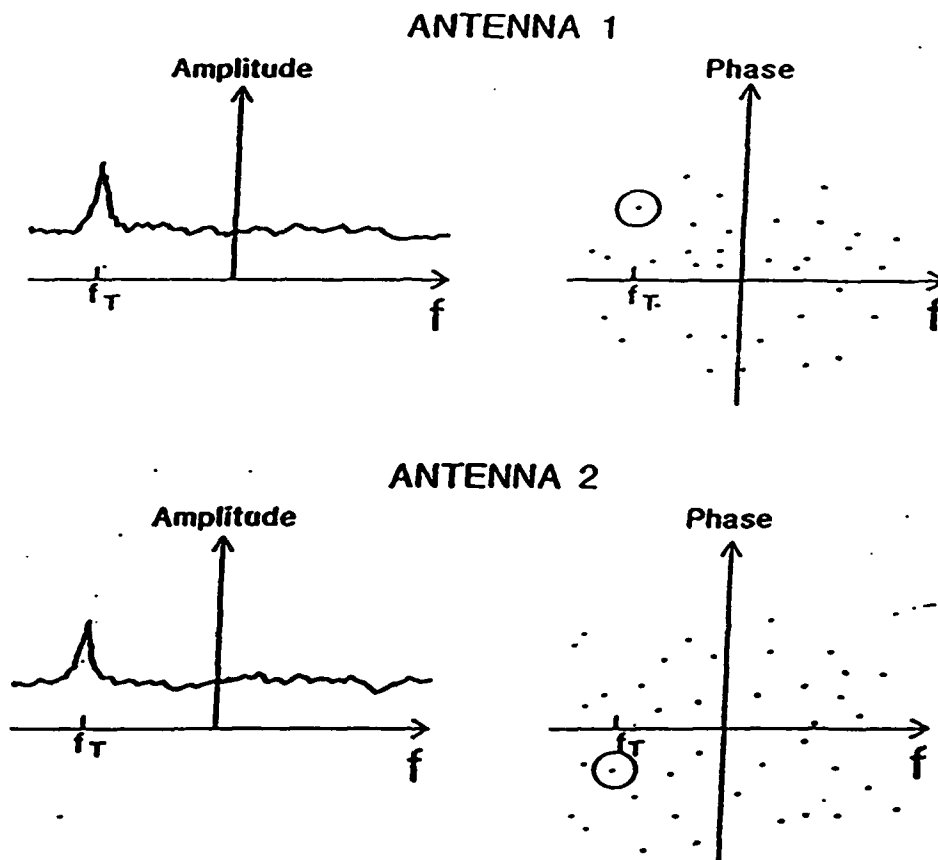


Fig. 4. Complex Fourier spectra for the two antennas in Figure 3, showing the signature of a single moving target. (From Adams, et al., 1985.)

Michael J. Volek
771 N. 500 E. Bsmt
Logan UT 84321
(801) 753-2148

19 August 1988

Dear Dr Balsley:

I am in the process of preparing my thesis in the Soil Science and Biometeorology Department at Utah State University. I hope to complete in the Spring of 1989.

I am requesting your permission to include the attached material as shown. I will include acknowledgment and/or appropriate citations to your work as shown and copyright and reprint rights information in a special appendix. The bibliographical citation will appear at the end of the manuscript as shown below. Please advise me of any changes you require.

Please indicate your approval of this request by signing in the space provided, attaching any other form or instruction necessary to confirm permission. If you charge a reprint fee for use of the material, please indicate it below as well. If you have any questions, please call me at the number above.

The attachment is a figure from a paper that you wrote that appeared in the preprint volume of the 18th Conference on Radar Meteorology.

I hope you will be able to reply immediately. If you are not the copyright holder, please forward my request to the appropriate person or institution.

Thank you for your cooperation.

Michael J. Volek

I hereby give permission to Michael J. Volek to reprint the following material in his thesis:

Balsley, B. B., 1978: Design considerations for coherent radar systems for probing the troposphere, stratosphere, and mesosphere. Preprint Volume, 18th Conference on Radar Meteorology, March 28-31, 1979, Atlanta, Georgia, 387-390.

B. B. Balsley

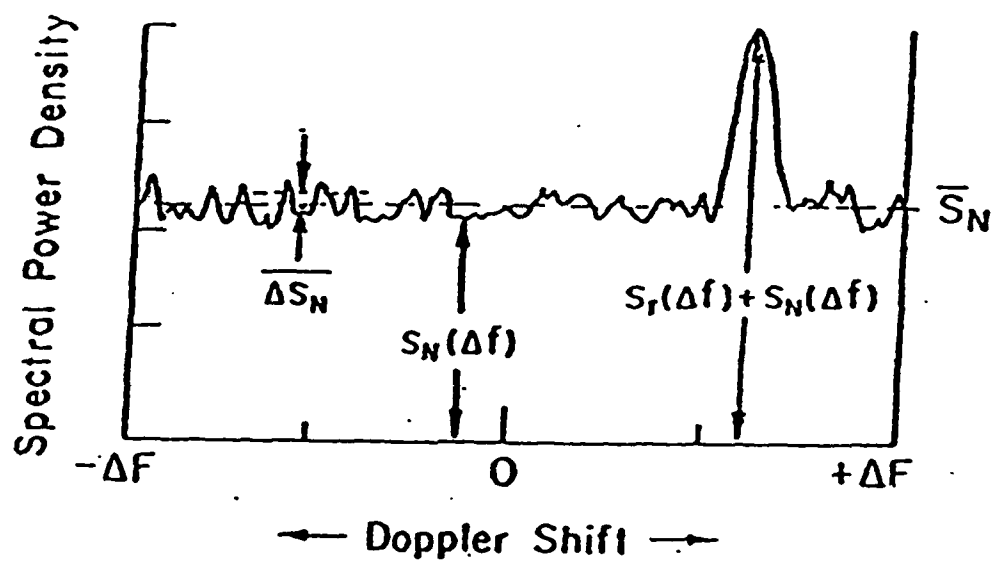


Fig. 2. Plot of spectral power density vs. Doppler shift. (From Balsley, 1978.)